



TITLE:

Effects of partial meridional barriers on the Antarctic Circumpolar Current(Dissertation_全文)

AUTHOR(S):

Ishida, Akio

CITATION:

Ishida, Akio. Effects of partial meridional barriers on the Antarctic Circumpolar Current. 京都大学, 1994, 博士(理学)

ISSUE DATE:

1994-05-23

URL:

<https://doi.org/10.11501/3096492>

RIGHT:

新 制
理
875
京大附図

学位申請論文

LION FILE

石田 明生

Effects of partial meridional barriers on the Antarctic Circumpolar Current

(南極周極流に対する部分的な子午線境界の効果)

石田 明生

Effects of partial meridional barriers
on the Antarctic Circumpolar Current
– Wind-driven barotropic model –

Akio Ishida

Abstract

The structure and transport of the Antarctic Circumpolar Current are examined by means of a simple barotropic model. We investigate the effects of a partial meridional barrier corresponding to the South American peninsula and the island arc which overlaps meridionally with the barrier. The island arc is modeled as another meridional barrier.

The transport is given by the ratio of the pressure difference produced by wind stress to the resistance resulting from bottom friction. In the limiting case with no friction, the pressure difference is determined by the magnitude of the wind stress at the latitudes of the ends of two meridional barriers, while the resistance is proportional to the difference between the Coriolis parameters at the same sites. The transport predicted by the model is reasonable as compared to the observed value. This suggests that the mechanism discussed in this paper can be applied to the real ocean.

We also find the relationship between the transport and the topographic drag on the meridional barriers. The time change of the transport is determined by the drag on the meridional barriers, the bottom stress, and the rate at which momentum is supplied by wind stress. The transport lags wind stress by several days.

1 Introduction

The Southern Ocean or Antarctic Ocean is the only zonally unbounded region within the world ocean. The Antarctic Circumpolar Current (ACC) flows eastward in the region. The transport of the current is about 130Sv ($1 \text{ Sv} = 10^{12} \text{ cm}^3\text{s}^{-1}$), which is much greater than that of other ocean currents (e.g. Whitworth et al., 1982; Whitworth, 1983). Although numerous studies have attempted to find the dynamics that determine the transport of the ACC, those dynamics remain unclear (Nowlin and Klinck, 1986).

Hidaka and Tsuchiya (1953) constructed models of the ACC as a laterally viscous zonal stream driven by surface wind stress. In order to limit the total transport of the ACC to observed values, a lateral eddy viscosity of more than $10^{10}\text{cm}^2\text{s}^{-1}$ is required by their models — several orders of magnitude greater than that generally envisaged in other oceanic currents. Subsequently, attempts have been made to describe a model of the dynamics of the ACC that predicts a transport independent of the friction coefficient.

Munk and Palmen (1951) suggested that drag due to bottom topography provides sufficient retarding force on the flow to balance the surface wind forcing. Gill and Bryan(1971) developed a primitive equation, three-dimensional numerical model of the ocean. In their experiments the combined action of topography and baroclinicity increased the transport.

In recent years, a downward transfer of wind-imparted zonal momentum by synoptic eddies has been proposed. Studies using an eddy-resolving quasi-geostrophic numerical model have been carried out (McWilliams et al., 1979; Treguier and McWilliams, 1989; Wolff and Olbers, 1989; Wolff et al., 1991). In these experiments the momentum input by wind stress is transferred to the lowest layer by eddy activity, where it may leave the system by bottom form drag. The bottom form drag

thus provides sufficient retarding force on the flow to balance the surface wind forcing. However the effects of lateral topography (e.g. the South American peninsula and an island arc to the east) are not sufficiently represented in these experiments. So, it is not clear if bottom form drag is the only mechanism that balances the surface wind forcing.

Although all of the above studies regard the ACC as a purely zonal phenomenon, Stommel (1957) and Gill (1968) pointed out the effects of lateral topography. Stommel observed that although Drake Passage is quite broad and deep, the flow through Drake Passage is blocked by an island arc to the east and the ACC therefore cannot be purely zonal. He suggested the possibility that 'the ACC is essentially amenable to treatment by the Sverdrup theory; that the current is essentially frictionless except in a narrow region just after it passes through Drake Passage.' Stommel (1962) later constructed a model that treated Drake Passage as a porous barrier in a meridional wall, but he did not state the physical meaning of the porous barrier.

Gill (1968) examined in detail the effects of a partial meridional barrier with a gap corresponding to Drake Passage. The transport was determined to be the ratio of eastward wind stress to bottom stress on the first order dynamics of his model. Gill found that large values of vertical or horizontal friction were needed to keep the model transport to a reasonable value. (He cited a vertical friction coefficient of $10^3 \text{cm}^2 \text{s}^{-1}$ and a horizontal friction coefficient of $10^8 \text{cm}^2 \text{s}^{-1}$.)

Klinck (1986) ran a barotropic numerical model to study the effects of the island arc suggested by Stommel (1957). He modeled the island arc as a partial barrier and showed the dependence of the transport of the ACC on the lengths of the two meridional barriers. As the results of his experiments, he showed that as the two barriers' overlapping length increased, the transport decreased. However, he did not show how the barriers retarded the model current.

The main objective of this paper is to describe the effects of a partial meridional barrier and of an island arc. The problem to be considered, then, is how their effects control the transport of the ACC, and, furthermore, how the momentum input by wind stress is retarded. The bottom form drag mentioned previously also seems to be important in the balance of momentum. However, we can acquire the whole image only after resolving each element of the physical process. We therefore consider only the effects of lateral topography.

2 Formulation

The bottom topography near Drake Passage is shown in Fig. 1, where the South Sandwich Islands and South Georgia Island are part of an island arc. Peterson and Whitworth(1989) suggested a schematic view of the ACC in which it is deflected north over the Falkland Plateau after passing through Drake Passage and moves along the northern flank of the Ewing Bank and the Falkland ridge.

Stommel (1957) modeled the South American peninsula and the island arc as two partial meridional barriers. He emphasized that the ACC cannot be purely zonal, namely, that there is no latitude band without a meridional barrier. However, if we regard the island arc, the Ewing Bank and the Falkland ridge as the second meridional barrier, the South American peninsula and the barrier overlap in the latitude band from about 50°S to 57°S . It is expected that the western boundary current develops in the latitude band, where momentum is dissipated. We then use the geometry shown in Fig. 2. The model is a zonal channel with two meridional barriers. The geometry appears to be the simplest that can include the above features.

A rectangular coordinate system is used with x, y and z measuring distances eastward, northward and upward respectively. The origin corresponds to a point at the southern end of Drake Passage. The lines $x = 0$ and $x = L_x$ represent the same

meridian, the section $y > y_1$ being a barrier similar to the South American peninsula. The line $x = l_x$ represents the second meridional barrier, which corresponds to the island arc. The latitudes at $y = y_1$ and y_2 represent those at the southern end of the South American peninsula and at the northern flank of the Ewing Bank, respectively. The geometry shown in Fig. 2 is basically the same as that used by Gill (1968). However, he did not include the second meridional barrier.

Dynamically, the model is essentially that used by Stommel (1948). The ocean is assumed to be homogeneous and of constant depth, H , and the horizontal momentum equations are integrated over this depth. If u and v are the eastward and northward velocity components and ρ the density, the mass transport components are defined by

$$U = \int_{-H}^0 \rho u dz, \quad V = \int_{-H}^0 \rho v dz,$$

and the integral of the pressure p is also defined by

$$P = \int_{-H}^0 p dz.$$

Following Stommel (1948), a linear friction law is assumed so that the vertically integrated equations have the form

$$-fV = -\frac{\partial P}{\partial x} + \tau^x - \nu U, \quad (1)$$

$$fU = -\frac{\partial P}{\partial y} + \tau^y - \nu V, \quad (2)$$

where f is the Coriolis parameter given by $f = f_0 + \beta y$ (β is constant), τ^x and τ^y are the eastward and northward components of wind stress, respectively, and ν is the coefficient of friction.

From the continuity requirement, a transport stream function ψ is defined by

$$\frac{\partial \psi}{\partial y} = -U, \quad \frac{\partial \psi}{\partial x} = V.$$

Substitution in (1) and (2), and elimination of P , leads to

$$\nu \nabla^2 \psi + \beta \frac{\partial \psi}{\partial x} = \text{curl} \tau, \quad (3)$$

where $\nabla^2 = \partial^2/\partial x^2 + \partial^2/\partial y^2$

The boundary conditions are that there must be no flux across solid boundaries, that is, that ψ must be constant on solid boundaries. The value of the constant can be set to zero on the northern boundaries ($x = 0, x = L_x$ and $y = L_y$), but ψ will have a different value on the southern boundaries ($x = l_x$ and $y = 0$). This value is a measure of the total transport through the channel and will be designated Q .

Now ψ_0 and ψ_1 are defined as the solution of the equations

$$\nu \nabla^2 \psi_0 + \beta \frac{\partial \psi_0}{\partial x} = \text{curl} \tau, \quad (4)$$

$$\nu \nabla^2 \psi_1 + \beta \frac{\partial \psi_1}{\partial x} = 0. \quad (5)$$

We solve (4) with the condition $\psi_0 = 0$ on all boundaries and solve (5) with the condition $\psi_1 = 0$ on the northern boundaries, and $\psi_1 = 1$ on the southern boundaries. The solution of (3) is then given by

$$\psi = \psi_0 + Q\psi_1. \quad (6)$$

ψ_0 represents the flow field driven only by the curl of the wind stress. The transport of this flow through the channel is zero. On the other hand, the flow field of ψ_1 is independent of the forcing, i.e., of the wind stress.

The total transport Q is given by substituting (6) in (1) and (2), and by integrating the momentum equations around the channel. Here the notations

$$(U_i, V_i) = \left(-\frac{\partial \psi_i}{\partial y}, \frac{\partial \psi_i}{\partial x}\right),$$

$$I_i = \oint [U_i dx + V_i dy], \quad J_i = \oint [-f V_i dx + f U_i dy] \quad (i = 0, 1),$$

are introduced. Since the pressure term is zero due to the continuity of pressure, Q is given by

$$Q = \frac{\oint[\tau^x dx + \tau^y dy] - (\nu I_0 + J_0)}{\nu I_1 + J_1}, \quad (7)$$

where νI_0 and νI_1 are the frictional force acting on the flow along the path of integration. J_0 and J_1 are the Coriolis forces on the flow across the path.

The solution ψ_1 of the homogeneous equation (5) represents the flow field driven by a wind stress whose curl is zero. Although ψ_1 depends on the geometry of the model basin and on the parameters ν and β , it is independent of the distribution of wind stress. Therefore, $\nu I_1 + J_1$ can be regarded as the resistance on a unit volume of the free flow defined by ψ_1 to which relative vorticity is not supplied. The numerator of R.H.S. of (7) is the driving force, which generates the total transport of the current through the channel. This can be interpreted as the pressure difference across the boundary established at Drake Passage. It is discussed in Section 4.

The flow defined by ψ_0 is driven only by $\text{curl}\tau$ and is independent of τ itself. If τ^x increases to $\tau^x + \tau_0$ (τ_0 is constant), the transport increases by $\tau_0 L_x / (\nu I_1 + J_1)$. This is a general result independent of the detail of the basin geometry (e.g. whether or not the meridional barriers overlap.) This suggests that not only the distribution but also the absolute value of the wind stress affects the transport of the ACC.

3 Solution for Low Friction

The problem of finding solutions analytically is not as straightforward as it might be because of the unusual geometry involved. The objective of this section is to find the functions ψ_1 and ψ_0 on the assumption that the value of the friction coefficient ν is small, similar to the assumption in Gill (1968). The whole basin can be divided into the sub-regions shown in Fig. 3, because the dominant vorticity balance is different in each sub-region. There are zonal jets in regions A and A' Regions B

and B' correspond to the western boundary layers. The Sverdrup solution is a good approximation in regions C and C'. Regions D and D' are required to represent the flow around the ends of the meridional barriers. Since regions D and D' have the scale of $O(\nu/\beta)$, the solutions for these regions do not affect the transport of the current. Thus we need not find the solutions for regions D and D'. The path of the line integral in (7) is chosen along the path PQRSP in Fig. 4.

If the lines $y = 0$ and $y = L_y$ are regarded as solid boundaries, boundary layers are formed near the lines. Here we assume the Sverdrup balance on the lines $y = 0$ and L_y and remove the influence of the boundaries. The flow field near Antarctica is not represented correctly due to this assumption. However, the flow near the path PQRSP chosen for line integral is not affected, because it is apart from the boundary. Though the flow near $y = 0$ may not be derived correctly, the transport and the structure of the ACC are not affected by this assumption.

3.1 Homogeneous Solution

In this sub-section we find the function ψ_1 defined by the homogeneous equation (5) and calculate the denominator $(\nu I_1 + J_1)$ in (7). The solutions in regions C and C' (ψ_{1C} and $\psi_{1C'}$) are that $\psi_{1C} = 1$ and $\psi_{1C'} = 0$, from the Sverdrup balance. Thus there must be zonal jets in regions A and A' to match the solution in region C with that in region C'. There are western boundary currents in regions B and B'.

As $\nu \rightarrow 0$, the solution in region A tends to a solution of the parabolic equation,

$$\nu \frac{\partial^2 \psi_{1A}}{\partial y^2} + \beta \frac{\partial \psi_{1A}}{\partial x} = 0, \quad (8)$$

where ψ_{1A} represent ψ_1 in region A.

If the co-ordinates defined by

$$\xi = l_x - x, \quad \eta = y - y_2 \quad (9)$$

are introduced, the equation (8) becomes

$$\frac{\partial \psi_{1A}}{\partial \xi} = \alpha \frac{\partial^2 \psi_{1A}}{\partial \eta^2}, \quad (10)$$

where $\alpha \equiv \nu/\beta$ (α is a measure of width of the western boundary current), the boundary condition at $\xi = 0$ is

$$\psi_{1A}(0, \eta) = \begin{cases} 0 & \eta > 0, \\ 1 & \eta < 0. \end{cases} \quad (11)$$

The solution of (10) is given by

$$\psi_{1A}(x, y) = \frac{1}{2} \operatorname{erfc}\left(\frac{y - y_2}{w_1(x)}\right), \quad (12)$$

where

$$w_1(x) = 2[\alpha(l_x - x)]^{1/2}, \quad \operatorname{erfc}(x) = \frac{2}{\sqrt{\pi}} \int_x^\infty e^{-t^2} dt.$$

In a similar manner, in deriving (12), the solution in region A' is given by

$$\psi_{1A'}(x, y) = \frac{1}{2} \operatorname{erfc}\left(\frac{y - y_1}{w_2(x)}\right). \quad (13)$$

where

$$w_2(x) = 2[\alpha(L_x - x)]^{1/2}$$

The widths of the zonal jets in regions A and A' are $O([\alpha(l_x - x)]^{1/2})$ and $O([\alpha(L_x - x)]^{1/2})$, respectively. They spread in proportion to $\alpha^{1/2}$. If the width of the zonal jets is larger than the overlapping length $\delta (\equiv y_2 - y_1)$ of the two meridional barriers, the boundary condition (11) will not be valid. Therefore δ should be longer than the width of the jets, i.e., $\delta > \max([\alpha l_x]^{1/2}, [\alpha(L_x - l_x)]^{1/2})$. If the condition is rewritten to that for the friction coefficient, $\nu < \min(\beta \delta^2 / l_x, \beta \delta^2 / (L_x - l_x))$. The solutions are valid for a friction coefficient small enough to satisfy this condition. If we set the parameters $\beta = 10^{-13} \text{ cm}^{-1} \text{ s}^{-1}$, $\delta = 1000 \text{ km}$, $L_x = 20000 \text{ km}$ and $l_x = 2000 \text{ km}$, to estimate the condition approximately, the constraint is rewritten to that for the

width of western boundary current, $\nu/\beta < 56$ km. The width of western boundary current represented in this model is comparable with the observed one, though it is slightly narrower.

In region B, the western boundary layer of thickness of $O(\nu/\beta)$ develops and the solution tends to a solution of

$$\alpha \frac{\partial^2 \psi_{1B}}{\partial x^2} + \frac{\partial \psi_{1B}}{\partial x} = 0. \quad (14)$$

The appropriate solution ψ_{1B} satisfying the conditions that $\psi_{1A} + \psi_{1B} = 0$ at $x = 0$, $y > y_1$ and $\psi_{1B} \rightarrow 0$ for $x \rightarrow \infty$ is

$$\psi_{1B}(x, y) = -\frac{1}{2} e^{-x/\alpha} \operatorname{erfc}\left(\frac{y - y_2}{w_1(0)}\right) \cdot \theta(y - y_1), \quad (15)$$

where

$$\theta(t) = \begin{cases} 0 & t < 0, \\ 1 & t > 0. \end{cases}$$

Similarly the solution in region B' is

$$\psi_{1B'}(x, y) = \left[1 - \frac{1}{2} \operatorname{erfc}\left(\frac{y - y_1}{w_2(l_x)}\right)\right] e^{(l_x - x)/\alpha} \cdot \theta(y_2 - y). \quad (16)$$

The resistance $\nu I_1 + J_1$ is calculated by using the above solutions. νI_1 is given by

$$\begin{aligned} \nu I_1 &= \nu \left(\int_P^Q \frac{\partial \psi_{1B}}{\partial x} dy - \int_Q^R \frac{\partial \psi_{1A}}{\partial y} dx + \int_R^S \frac{\partial \psi_{1B'}}{\partial x} dy - \int_S^P \frac{\partial \psi_{1A'}}{\partial y} dx \right) \\ &= \nu (I_{1B} + I_{1A} + I_{1B'} + I_{1A'}), \end{aligned} \quad (17)$$

where

$$\nu I_{1A} = \left(\frac{\nu \beta l_x}{\pi} \right)^{1/2}, \quad (18)$$

$$\nu I_{1A'} = \left(\frac{\nu \beta (L_x - l_x)}{\pi} \right)^{1/2}, \quad (19)$$

$$\nu I_{1B} = \frac{\beta \delta}{2} \operatorname{erfc}\left(-\frac{\delta}{w_1(0)}\right) + \left(\frac{\nu \beta l_x}{\pi} \right)^{1/2} \left[\exp\left(-\frac{\delta^2}{w_1(0)^2}\right) - 1 \right], \quad (20)$$

$$\nu I_{1B'} = \frac{\beta \delta}{2} \left[2 - \operatorname{erfc}\left(\frac{\delta}{w_2(l_x)}\right) \right] + \left(\frac{\nu \beta (L_x - l_x)}{\pi} \right)^{1/2} \left[\exp\left(-\frac{\delta^2}{w_2(l_x)^2}\right) - 1 \right]. \quad (21)$$

The terms νI_{1A} and $\nu I_{1A'}$ represent the frictional force acting on the zonal jets in regions A and A', while νI_{1B} and $\nu I_{1B'}$ represent that on the western boundary currents in regions B and B'. The frictional force is proportional to (friction coefficient ν)/(width of jet). Since the widths of the zonal jets are proportional to $\nu^{1/2}$, the frictional force is proportional to $\nu^{1/2}$. On the other hand, since the width of the western boundary current is $O(\nu/\beta)$, the frictional force does not strongly depend on ν . However, since the widths of the zonal jets broaden toward the western boundaries due to friction, the frictional force acting on the western boundary currents becomes small (the second terms of R.H.S. in eqs. (20) and (21)). These terms include those which set off the friction force on the zonal jet((18) and (19)).

Since there is no normal flow across the lines PQ and RS, the Coriolis term J_1 is given by

$$\begin{aligned} J_1 &= -f(y_2) \int_0^{l_x} \frac{\partial \psi_1}{\partial x} \Big|_{y=y_2} dx - f(y_1) \int_{l_x}^{L_x} \frac{\partial \psi_1}{\partial x} \Big|_{y=y_1} dx \\ &= -[f(y_1) - f(y_2)] = -\beta\delta. \end{aligned} \quad (22)$$

From the equations (17)~(21) and (22),

$$\begin{aligned} \nu I_1 + J_1 &= \frac{\beta\delta}{2} [\text{erfc}(-\frac{\delta}{w_1(0)}) - \text{erfc}(\frac{\delta}{w_2(l_x)})] \\ &+ \beta(\frac{\alpha}{\pi})^{1/2} [\sqrt{l_x} \exp(-\frac{\delta^2}{w_1(0)^2}) + \sqrt{L_x - l_x} \exp(-\frac{\delta^2}{w_2(l_x)^2})]. \end{aligned} \quad (23)$$

The resistance $\nu I_1 + J_1$ includes a term which is proportional to $\beta\delta$, which has the finite value $\beta\delta$ in the limit of $\nu \rightarrow 0$. This result suggests a mechanism that earlier models did not include and also shows that the island arc plays an important role in the transport by the ACC.

3.2 Nonhomogeneous Solution

Now we attempt to find the function ψ_0 defined by the nonhomogeneous equation (4) and calculate the numerator in R.H.S. of (7). The meridional component of the

wind stress is neglected because it is smaller than the zonal component. Moreover, the wind stress distribution is presumed to be uniform in a zonal direction.

In regions C and C', the Sverdrup solutions are good approximations. If the wind stress curl at $y = y_2$ and $y = y_1$ does not disappear, zonal jets will develop in regions A and A'. Western boundary currents exist in regions B and B'. The dominant vorticity balance is the same as that in the case of ψ_1 .

The solution when $0 \leq x < l_x$ is given by

$$\begin{aligned}\psi_0(x, y) = & \frac{1}{\beta} \frac{\partial \tau^x}{\partial y} \left\{ l_x - x + \frac{L_x - l_x}{2} \operatorname{erfc}\left(-\frac{y - y_2}{w_1(x)}\right) \right. \\ & \left. - e^{-x/\alpha} \left[l_x + \frac{L_x - l_x}{2} \operatorname{erfc}\left(-\frac{y - y_2}{w_1(0)}\right) \right] \cdot \theta(y - y_1) \right\},\end{aligned}\quad (24)$$

while the solution when $l_x < x < L_x$ is given by

$$\begin{aligned}\psi_0(x, y) = & \frac{1}{\beta} \frac{\partial \tau^x}{\partial y} \left\{ L_x - x + \frac{l_x}{2} \operatorname{erfc}\left(\frac{y - y_1}{w_2(x)}\right) \right. \\ & \left. - e^{(l_x - x)/\alpha} \left[L_x - l_x + \frac{l_x}{2} \operatorname{erfc}\left(\frac{y - y_1}{w_2(l_x)}\right) \right] \cdot \theta(y_2 - y) \right\}.\end{aligned}\quad (25)$$

Details of the derivation of (24) and (25) are given in the Appendix.

The term $\nu I_0 + J_0$ is calculated by using these solutions. Since the transport of the current ψ_0 is zero, J_0 is zero. Therefore, only νI_0 is required, and it becomes

$$\nu I_0 = (L_x - 2l_x)[\tau^x(y_1) - \tau^x(y_2)] - N M_2 - N M_3, \quad (26)$$

where

$$N M_2 = -\frac{L_x - l_x}{2} \frac{\partial \tau^x(y_2)}{\partial y} \left[\delta \operatorname{erfc}\left(\frac{\delta}{w_1(0)}\right) - 2\left(\frac{\alpha l_x}{\pi}\right)^{1/2} \exp\left(-\frac{\delta^2}{w_1(0)^2}\right) \right] \quad (27)$$

$$+ \frac{l_x}{2} \frac{\partial \tau^x(y_1)}{\partial y} \left[\delta \operatorname{erfc}\left(\frac{\delta}{w_2(l_x)}\right) - 2\left(\frac{\alpha(L_x - l_x)}{\pi}\right)^{1/2} \exp\left(-\frac{\delta^2}{w_2(l_x)^2}\right) \right],$$

$$N M_3 = \frac{\alpha L_x l_x}{2} \frac{\partial^2 \tau^x(y_2)}{\partial y^2} + \frac{\alpha L_x (L_x - l_x)}{2} \frac{\partial^2 \tau^x(y_1)}{\partial y^2}. \quad (28)$$

The first term in the R.H.S. of (26) is the frictional force acting on the western boundary current, according to Sverdrup's theory and independent of ν . $N M_2$ is the

frictional force on the western boundary currents, formed by the zonal jets in regions A and A'. The zonal jets are generated because the value of the wind stress curl at $y = y_2$ and $y = y_1$ is not zero. NM_3 is the frictional force on the zonal jets in regions A and A'

The line integral of the wind stress is given by

$$\oint \tau^x dx = \tau^x(y_1)(L_x - l_x) + \tau^x(y_2)l_x. \quad (29)$$

From (26) and (29), the numerator in (7) is given by

$$NM = NM_1 + NM_2 + NM_3, \quad (30)$$

where

$$NM_1 = \tau^x(y_1)l_x + \tau^x(y_2)(L_x - l_x). \quad (31)$$

NM_1 in (30) is dominant in the appropriate range of parameters. Therefore the values of the wind stress on lines PS' and R'Q' are more important than those on the lines QR and SP' along which zonal jets flow. This is due to the frictional force on the western boundary currents driven by $\text{curl}\tau$; a physical explanation is given in Section 4. The points P', Q', R' and S' are located just west of points P, Q, R and S across a meridional boundary (see Fig. 4).

4 Physical Interpretation of the Solution

The transport prediction equation (7) is composed of the terms (23) and (30). Although equation (7) is so complicated, it has a simple form in the limiting case with no friction ($\nu \rightarrow 0$ i.e. $\alpha \rightarrow 0$), that is

$$Q = \frac{\tau^x(y_1)l_x + \tau^x(y_2)(L_x - l_x)}{\beta\delta} \quad (32)$$

The purpose of this section is to provide a physical interpretation of this formula.

If Drake Passage is presumed to be closed by a meridional barrier, the pressure difference across the barrier is caused by the surface wind stress. Then, if the barrier is removed, the flow through Drake Passage is generated and the transport of the flow is determined by the resistance on the flow. The resistance equals to the pressure decrease resulting from the free flow ψ_1 . So we first investigate how the pressure difference across Drake Passage is generated. Next, we find the pressure decrease along with the free flow ψ_1 .

4.1 Pressure Difference induced by Wind Stress

Now we consider the pressure difference across Drake Passage, which is presumed to be closed by a meridional barrier. If the equations of motion are integrated along the path PQRSP', the pressure difference between P and P' may be determined. The northward velocity V on the path PQ is $(l_x/\nu)\partial\tau^x/\partial y$, if V is assumed to be the Sverdrup transport divided by the width ν/β of western boundary layer. Similarly, $V = (L_x - l_x)/\nu\partial\tau^x/\partial y$ along path RS. The Coriolis force is zero, because the transport through the channel is set at zero because of the inclusion of the barrier in Drake Passage. Integration along each path leads to

$$P_Q - P_P = -[\tau^x(y_2) - \tau^x(y_1)]l_x, \quad (33)$$

$$P_R - P_Q = \tau^x(y_2)l_x, \quad (34)$$

$$P_S - P_R = -[\tau^x(y_1) - \tau^x(y_2)](L_x - l_x), \quad (35)$$

$$P_{P'} - P_S = \tau^x(y_1)(L_x - l_x). \quad (36)$$

The sum of these equations yields

$$P_{P'} - P_P = \tau^x(y_1)l_x + \tau^x(y_2)(L_x - l_x). \quad (37)$$

Equation (37) is equal to the numerator in (32). Thus this pressure difference can be interpreted as the driving force of the transport through the passage.

It should be noted that the terms including $\tau^x(y_2)$ in (33) and (34) and the terms including $\tau^x(y_1)$ in (35) and (36) cancel each other. Since the pressure gradient along the eastern boundary becomes zero due to the β -effect in the case of $\tau^y = 0$, the pressure difference between P and R is determined only by the difference between P and S'. The difference between R and P' is also determined only by that between R and Q'. The first term of the R.H.S. of (37) is the pressure difference between P and S', and the second term is that between R and Q'.

However the above discussion is not correct, if the meridional component of the wind stress is not zero. If the meridional component is included, the pressure difference between P and P' is given by

$$P_{P'} - P_P = \oint_{PS'R'Q'P'} \tau \cdot dl, \quad (38)$$

where dl is the line-element along the path $PS'R'Q'P'$. The pressure difference between S' and R' is given by $\int_{S'}^{R'} \tau^y dy$, while that between Q' and P' is given by $\int_{Q'}^{P'} \tau^y dy$. Thus the meridional component of the wind stress also affects the transport through the channel.

The equation (38) represents that the pressure difference between P and P' equals to the line integral of wind stress along the path $PS'R'Q'P'$. Although the pressure difference is derived from the line integral along the path $PQRSP'$ in this subsection, the same result can also be derived from that along the path $PS'R'Q'P'$. The result is independent of the integration path, because pressure is conservative force.

If the wind stress is uniform eastward ($\tau^x = \tau_0$, $\tau^y = 0$), there is no flow, and the stress balances with the purely zonal pressure gradient force. The pressure difference across the barrier at $x = 0$ is then $\tau_0 L_x$.

4.2 Pressure Decrease resulting from free flow ψ_1

We consider the situation that the barrier presumed in the previous subsection is removed and investigate the pressure decrease resulting from free flow ψ_1 with the transport Q . Since the velocity along the paths PQ and RS is given by $\beta Q/\nu$, and the transport across the paths QR and SP' is Q , the pressure differences are given by

$$P_Q - P_P = -\beta\delta Q, \quad (39)$$

$$P_R - P_Q = f(y_2)Q, \quad (40)$$

$$P_S - P_R = -\beta\delta Q, \quad (41)$$

$$P_{P'} - P_S = -f(y_1)Q. \quad (42)$$

These equations show that the pressure decrease along the western boundaries is $2\beta\delta Q$ (eqns. (39) and (41)), and the pressure increase due to the Coriolis force is $\beta\delta Q$ (eqns. (40) and (42)). The sum of the equations gives

$$P_{P'} - P_P = -2\beta\delta Q + [f(y_2) - f(y_1)]Q = -\beta\delta Q. \quad (43)$$

The transport Q of the current is determined, as the pressure difference given by (37) is cancelled by the pressure change given by (43). That is,

$$\beta\delta Q = \tau^x(y_1)l_x + \tau^x(y_2)(L_x - l_x). \quad (44)$$

This equation is the same as (32). $\beta\delta$ in (44) is the resistance on a unit volume of the flow through the channel that has the meridional barriers with the overlapping length δ . The value $\beta\delta$ is independent of ν , because the width of the western boundary current is proportional to ν . As ν decreases, the width becomes narrower. The resistance thus does not change. The transport is determined as a result of the balance between the pressure difference and the resistance.

Stommel (1962) constructed a model that treated Drake Passage as a porous barrier. The physical meaning of the porous barrier settled by him is clear from (44). If

the current is essentially frictionless except in a narrow region near western boundary, the ACC must flow through the frictional western boundary with the length δ . Therefore the porous barrier is interpreted as the frictional western boundary, which has the resistance $\beta\delta$.

Equation (32) is the same as equation (12) in Godfrey (1989) and equation (52) in Minato and Kimura (1980). These studies found the circulation around Australasia and Japan to be driven by wind stress. Their models differ from the one in the present study in that equation (32) predicts non-zero transport even by wind stress with a curl of zero.

5 Results

The dependence on parameters of the solution derived in section 3 is now discussed. The structure of the solution depends on the friction coefficient ν , the distribution of the wind stress and the geometry of the model basin. In order to clarify the effects of partial meridional barriers on the ACC, the dependence on the geometry is also investigated. The transport of the current is given by the ratio of the driving force (30) to the resistance (23). The driving force (the numerator) depends on the distribution of wind stress but the resistance (the denominator) does not. The dependence of these two terms on appropriate parameters is also investigated.

5.1 Resistance to Flow

The driving force (30) is $O(\tau_0 L_x)$, if the typical wind stress magnitude is τ_0 . For an intuitive understanding, we investigate the dependence on parameters of the transport instead of the resistance (the denominator), provided that the numerator is fixed at $\tau_0 L_x$. The first term in (23) is $O(\beta\delta)$, while the second term is less than $O(\beta\delta)$ for $\delta > \max((\alpha l_x)^{1/2}, [\alpha(L_x - l_x)]^{1/2})$ (see Section 3). The first term is therefore

dominant. The denominator $\nu I_1 + J_1$ depends on the friction coefficient ν and the geometry of the basin. The geometry is characterized by the overlapping length δ and the distance l_x between two meridional barriers. We investigate the dependence of the transport on these two factors using ν as a parameter.

Figure 5 shows the transport as a function of δ , where $\beta = 10^{-13} \text{ cm}^{-1}\text{s}^{-1}$, $L_x = 20000\text{km}$, $l_x = 2000\text{km}$, and $\tau_0 = 1 \text{ dyn}\cdot\text{cm}^{-2}$. The thick line represents the transport in the limiting case with no friction ($\nu \rightarrow 0$), and is given by $\tau_0 L_x / \beta \delta$. As ν increases, the transport decreases. However, as δ increases, the curves approach the curve representing the limit with no friction, and thus the dependence on ν becomes small. This fact shows that as δ increases, the frictional force on the western boundary current becomes dominant, because the dissipation of the western boundary current depends on a mechanism which is independent of ν .

Next we find the dependence of the transport on l_x . From the symmetry of equation (23), the value of the denominator is symmetrical about $l_x = L_x/2$. Figure 6 shows the transport to l_x when $\delta = 1000\text{km}$. The thick line shows the transport with zero friction, that is $\tau_0 L_x / \beta \delta$. The transport reaches a maximum when $l_x = L_x/2$. As $|l_x - L_x/2|$ increases, the transport becomes small, but the relationship is limited.

From the above results, it is found that there is resistance in proportion to δ and that the value is almost independent of l_x .

5.2 Driving Force

Following up on the previous subsection, we investigate the dependence of the transport on parameters with the denominator fixed at $\beta \delta$ for an intuitive understanding. The numerator depends on the distribution of wind stress relative to the basin geometry. The dependence of the numerator on the distribution of wind stress is then investigated, when the geometry is fixed ($L_x = 20000\text{km}$, $l_x = 2000\text{km}$,

$y_1 = 1000\text{km}, y_2 = 2000\text{km}$).

We estimate the order of the three terms NM_1, NM_2 and NM_3 in (30). NM_1 is $O(\tau_0 L_x)$. The terms in the parentheses in NM_2 are less than δ by one order for $\delta < (\alpha L_x)^{1/2}$, because the terms in the parentheses cancel each other. If the typical spatial scale of the wind stress is L_w , NM_2 is $O(\tau_0 L_x \cdot 0.1\delta/L_w)$. Thus NM_2 is less than NM_1 by more than one order for $\delta < L_w$. NM_3 is $O(\tau_0 L_x \cdot \alpha L_x/L_w^2)$ and is less than NM_1 by one order. Therefore, only NM_1 is the most dominant term and NM_3 affects the value of the numerator slightly.

The wind stress is assumed to have the following distribution

$$\tau^x(y) = \tau_0 \cos \frac{\pi(y - y_0)}{L_w}, \quad (45)$$

where $\tau_0 = 1 \text{ dyn} \cdot \text{cm}^{-2}$, and $L_w = 4000\text{km}$ are typical scales (Hellerman and Rosenstein, 1983). y_0 is the latitude where the zonal wind stress is a maximum.

Figure 7 shows the transport as a function of y_0 . The numbers in the figure correspond to the contributions from NM_1, NM_2 and NM_3 . As denoted above, NM_1 has a maximum amplitude, and also for $l_x \ll L_x - l_x$, the term $\tau^x(y_2)(L_x - l_x)$ in NM_1 is dominant. Therefore NM_1 reaches a maximum value when y_0 is near y_2 . On the other hand, since the term $[\alpha L_x(L_x - l_x)/2]\partial^2 \tau^x(y_1)/\partial y^2$ in NM_3 is dominant, NM_3 reaches a maximum when y_0 is near y_1 , and its sign is opposite to the sign of NM_1 . Figure 8 shows the total transport as a function of y_0 , when ν is chosen as a parameter. As ν increases, NM_3 increases and the total transport becomes different from the value predicted by NM_1 . However, since NM_3 is near zero when $y_0 \sim 3000\text{km}$, the transport depends little on ν in that case.

The range of the transport of the model ACC to the parameters is estimated to be from 95Sv to 330Sv, if the parameters are set as follows: $500 < \delta < 1000\text{km}$, $10^{-7} < \nu < 5 \times 10^{-7}\text{s}^{-1}$, and $2000 < y_0 < 3000\text{km}$. The upper limit is slightly larger, but in the order of the observed values (e.g. Whitworth et al., 1982). This result

shows that the model can represent the essential mechanisms of the ACC despite its simplicity.

5.3 Flow Pattern

The zonal means of the annual zonal wind stress have a maximum value near latitude 47°S (Hellerman and Rosenstein, 1983). This latitude corresponds to one that is somewhat north of the northern edge (50°S) of the Ewing Bank, and also to one somewhat north of latitude y_2 in the model basin. According to Fig. 2 in Johnson (1989), the zero curl latitude, i.e., the maximum eastward wind stress, varies from 40°S to 50°S . Thus the real distribution of the wind stress corresponds to the range of y_0 : $2000 < y_0 < 3000\text{km}$.

Figure 9 shows the flow patterns when $y_0 = 2000\text{km}$ (a) and 3000km (b). The transport in Fig. 9(a) is larger than that in Fig. 9(b), because $\tau^x(y_2)$ in (a) is larger than that in (b). Since the curl of the wind stress at latitude y_2 is zero in (a), a strong zonal jet exists in region $0 < x < l_x$. This reflects the structure of free flow $Q\psi_1$. In (b), there is a northward western boundary current along the boundary at $x = 0$, and the zonal flow elsewhere with a southward component. It has been well known that there seems to be a general southward component of the current over the entire southern ocean except just after it passes through Drake Passage (e.g. Deacon, 1937). It is because the transport through the passage is nearly the same as the Sverdrup transport in the latitude bands that $y_1 < y < y_2$. Since the free flow $Q\psi_1$ must be zonal due to the β -effect except in the western boundary region, it has a southward component at $x = l_x$. However, the western boundary current derived by Sverdrup's theory cancels the component of $Q\psi_1$, so that the total southward current at $x = l_x$ does not appear. Baker (1982) indicated that the transport predicted from the wind stress curl around 55°S (which is in the latitude band where the meridional

barriers' overlap) is much the same as the transport through Drake Passage. Thus it is suggested that the flow pattern in (b) is more real than the pattern in (a).

6 Topographic drag and transients

The eastward momentum balance in the model gives the relationship between the topographic drag on the meridional barriers and the transients of the transport of the ACC.

If the eastward momentum equation is integrated over the whole basin, the equation becomes

$$L_x \left(\frac{d}{dt} + \nu \right) Q + \iint \frac{\partial P}{\partial x} dx dy = \iint \tau^x dx dy, \quad (46)$$

where the pressure gradient term is the sum of the force on the barriers, i.e. the topographic drag. If the magnitude of the topographic drag and the wind stress is given, the transport fluctuations can be calculated by using (46). However the magnitude of the drag is a consequence of the forcing. So the drag depends on the pattern of the current and the magnitude of the transport. To avoid this difficulty, it is assumed that the pattern of the current is in steady state but the transport is not steady. This is equivalent to the assumption that the propagation speed of a barotropic Rossby wave is so fast that the propagation time can be neglected. The topographic drag term can be represented as a function of the transport Q on this assumption. Thus the transport fluctuations can be found by (46).

We find the drag on the meridional barrier at $x = 0$. If the width of the western boundary current can be approximated to be ν/β , the meridional momentum equation along the eastern coast ($x = 0^+$) is given by

$$\frac{\partial P(0^+, y)}{\partial y} = \begin{cases} -\beta Q - l_x \frac{\partial \tau^x}{\partial y} & y_1 < y < y_2 \\ -L_x \frac{\partial \tau^x}{\partial y} & y_2 < y < L_y \end{cases} \quad (47)$$

Since only the pressure difference across the barrier is necessary to find the drag, then

the pressure $P(0^-, y)$ on the western side of the barrier is set to zero. If equation (47) is integrated meridionally, the pressure on the eastern side is given by

$$P(0^+, y) = \begin{cases} -\beta Q(y - y_1) - l_x[\tau^x(y) - \tau^x(y_1)] & y_1 < y < y_2 \\ -\beta\delta Q - L_x\tau^x(y) + l_x\tau^x(y_1) + (L_x - l_x)\tau^x(y_2) & y_2 < y < L_y. \end{cases} \quad (48)$$

Thus the drag $F^{(1)}$ on the barrier at $x = 0$ is given by

$$\begin{aligned} F^{(1)} &= - \int_{y_1}^{L_y} P(0^+, y) dy \\ &= \beta\delta\left[\frac{\delta}{2} + L_y - y_2\right]Q + l_x \int_{y_1}^{y_2} \tau^x dy + L_x \int_{y_2}^{L_y} \tau^x dy \\ &\quad - l_x(L_y - y_1)\tau^x(y_1) - (L_x - l_x)(L_y - y_2)\tau^x(y_2). \end{aligned} \quad (49)$$

Similarly, the drag $F^{(2)}$ on the barrier at $x = l_x$ is given by

$$\begin{aligned} F^{(2)} &= \beta\delta\left[\frac{\delta}{2} + y_1\right]Q + (L_x - l_x) \int_{y_1}^{y_2} \tau^x dy + L_x \int_0^{y_1} \tau^x dy \\ &\quad - l_x y_1 \tau^x(y_1) - (L_x - l_x)y_2 \tau^x(y_2). \end{aligned} \quad (50)$$

The sum of both drag components is

$$F^{(1)} + F^{(2)} = \beta\delta L_y Q + L_x \int_0^{L_y} \tau^x dy - L_y[l_x\tau^x(y_1) + (L_x - l_x)\tau^x(y_2)], \quad (51)$$

which, when substituted into the pressure term of (46), yields

$$\left(\frac{d}{dt} + \nu + \frac{\beta\delta L_y}{L_x}\right)Q = \frac{L_y}{L_x}[l_x\tau^x(y_1) + (L_x - l_x)\tau^x(y_2)]. \quad (52)$$

If $\nu \ll \beta\delta L_y/L_x$, we obtain (32) in the steady state as the balance between the drag on the meridional barriers and the rate at which momentum is supplied by the wind stress.

Equation (52) represents the response of the transport to the time change in wind stress. If $\tau^x = \tau_0 e^{i\omega t}$, where ω is the frequency of wind fluctuations, (52) becomes

$$\left(\frac{d}{dt} + \frac{1}{T}\right)Q = \tau_0 L_y e^{i\omega t}, \quad (53)$$

where $T \equiv (\nu + \beta\delta L_y/L_x)^{-1}$. The solution is given by

$$Q = \frac{\tau_0 L_y T}{(1 + \omega^2 T^2)^{1/2}} e^{i(\omega t - \varphi)}, \quad (54)$$

where $\varphi = \tan^{-1}(\omega T)$. If the forcing period is much longer than T , the response has the same amplitude as that at the steady state and lags the forcing by T . At higher frequencies, the response is attenuated by a factor of $(1 + \omega^2 T^2)^{-1/2}$ and the time lag is reduced. The time lag is estimated to be from 4.6 days to 10.5 days, if the parameters in the previous section are set. This is comparable with the observations of Wearn and Baker (1980) who showed that the pressure difference across Drake Passage lagged the wind by about 9 days, and by Whitworth (1983) who showed that the transport lagged the wind by about 17 days. Peterson (1988) also derived that the pressure difference lagged the wind by about 14 days by comparisons of multilayer bottom pressure records with time series of the zonally averaged wind stress.

Wearn and Baker (1980) constructed a simple model similar to the one included in this paper. They introduced the dissipation in proportion to the transport and found that the transport lagged behind the wind by about 7 days. Although the physical mechanism of the dissipation was not given, it is represented in this model as the sum of bottom friction and topographic drag.

Both models are incomplete, as they exclude the mechanism of Rossby wave propagation. If this mechanism is included, the time lag will be longer than that predicted in the models. However, it is difficult to include the mechanism because of the unusual geometry included.

Rossby wave must propagate the distance L_x so as to spin up the flow field in the latitude bands that the meridional barriers don't overlap ($y < y_1$ and $y > y_2$). The propagation time around the Southern Ocean for a Rossby wave with the half wave length L_y is given by $\pi^2 L_x / \beta L_y^2$, which is about 14 days. This is comparable

with the time lag estimated above. On the other hand, Rossby wave must propagate the distance l_x ($0 < x < l_x$) and $L_x - l_x$ ($l_x < x < L_x$) in the latitude band that the barriers overlap ($y_1 < y < y_2$). Therefore the time required for the flow field to spin up in the region is much shorter than that in the other regions. The Rossby wave propagation time thus could be neglected in the latitude band that the meridional barriers overlap. It is left for future work to formulate the fluctuation of the transport through the channel including Rossby wave generation and propagation in the complex geometry.

7 Summary

The effects of two partial meridional barriers overlapping each other on the ACC were investigated, using a simple barotropic model. It was found that the transport is predicted by equations (7), (23) and (30). Equation (7) became (32) in the limiting case with no friction. Equation (32) is interpreted as the ratio of the pressure difference between the two sides of Drake Passage to the resistance $\beta\delta$. This shows that the friction acting on the western boundary current with length δ is given by $\beta\delta$ in the limiting case with no friction. The results provide a solution to the problem that large values of the friction coefficient are required to keep the model transport at a reasonable value.

The pressure difference is driven by the wind stress at the latitudes of the ends of the meridional barriers and it also drives the ACC. The distribution of wind stress curl is therefore not necessarily important for the determination of the transport. However, it influences the flow pattern. The model can represent the horizontal structure of the ACC, which has a northward boundary current just after moving through Drake Passage, and the southward current over the entire southern ocean.

The drag on the meridional barriers and the response of the ACC to wind fluc-

tuations were investigated. The momentum input by wind stress is balanced by the transient of the transport of the ACC, the drag on the meridional barriers, and the dissipation due to bottom friction. The response of the model ACC lags the fluctuations of the wind stress by several days due to the drag and the bottom friction. It is left for future work to study the process of the response of the ACC to forcing fluctuations associated with the generation and propagation of Rossby waves.

We have paid no attention to the probable disturbing effects of bottom topography within ocean basins. Because of the small stratification in the Southern Ocean, the flat bottom models are not as good as in subtropical gyres where a permanent pycnocline exists and insulates the wind driven flow from the bathymetry. The flat bottom models are useful to give order of magnitude estimates for processes but not sufficient for a realistic description of the transport. However, the main objective of the paper is to illustrate the process how partial meridional barriers control the transport of the ACC. The South American peninsula and the island arc to the east are most pronounced topography, thus the effects of them on the ACC is most important. More comprehensive models that can describe the effects of both lateral and bottom topography are required to illustrate a realistic description of the ACC.

Acknowledgments

This work was performed while the author was a student of the Department of Geophysics of Kyoto University. I would like to express my thanks to Prof. N. Imasato of the Department for suggesting the study and for his guidance throughout. I am also grateful to Dr. S. Sakai of Kyoto University for his valuable advice and encouragement. Thanks are extended to other members of the Department of Geophysics of Kyoto University for their helpful discussions.

Appendix A: Nonhomogeneous solution

Since the Sverdrup solution is a good approximation in regions C and C', the solutions ψ_{0C} and $\psi_{0C'}$ are given by

$$\psi_{0C} = \frac{l_x - x}{\beta} \frac{\partial \tau^x}{\partial y}, \quad \psi_{0C'} = \frac{L_x - x}{\beta} \frac{\partial \tau^x}{\partial y}. \quad (\text{A.1})$$

The vorticity equation in region A is the same as that for ψ_{1A} . The boundary condition is

$$\psi_{0A}(0, \eta) = \begin{cases} 0 & -\infty < \eta < 0 \\ \frac{L_x - l_x}{\beta} \frac{\partial \tau^x}{\partial \eta} & 0 < \eta < \infty, \end{cases}$$

from matching of the Sverdrup solution in region C'. The solution is given by

$$\psi_{0A} = \int_0^\infty \frac{L_x - l_x}{2\beta(\pi\alpha\xi)^{1/2}} \frac{\partial \tau^x}{\partial p} \exp\left(-\frac{(\eta - p)^2}{4\alpha\xi}\right) dp. \quad (\text{A.2})$$

We calculate this equation replacing $\partial \tau^x(p)/\partial p$ with $\partial \tau^x(0)/\partial p$ in the integrand, because the meridional scale of region A is much smaller than the spatial scale of the wind stress. The solution in $0 < x < l_x$ is given by

$$\psi_{0A}(x, y) = \frac{L_x - l_x}{2\beta} \frac{\partial \tau^x}{\partial y} \operatorname{erfc}\left(-\frac{y - y_2}{w_1(x)}\right). \quad (\text{A.3})$$

Similarly, the solution in region A' is given by

$$\psi_{0A'}(x, y) = \frac{l_x}{2\beta} \frac{\partial \tau^x}{\partial y} \operatorname{erfc}\left(-\frac{y - y_1}{w_2(x)}\right). \quad (\text{A.4})$$

The vorticity equation and the boundary conditions for ψ_{0B} are the same as those for ψ_{1B} . The solution is given by

$$\psi_{0B}(x, y) = -\frac{1}{\beta} \frac{\partial \tau^x}{\partial y} e^{-x/\alpha} \left[l_x + \frac{L_x - l_x}{2} \operatorname{erfc}\left(-\frac{y - y_2}{w_1(0)}\right) \right] \theta(y - y_1). \quad (\text{A.5})$$

In the same way, the solution in region B' is given by

$$\psi_{0B'}(x, y) = -\frac{1}{\beta} \frac{\partial \tau^x}{\partial y} e^{(l_x - x)/\alpha} \left[L_x - l_x + \frac{l_x}{2} \operatorname{erfc}\left(\frac{y - y_1}{w_2(0)}\right) \right] \theta(y_2 - y). \quad (\text{A.6})$$

We find $\nu I_0 + J_0$ using the above solutions. Since the transport by the flow ψ_0 is zero, J_0 is zero. I_0 is found from the equation

$$\begin{aligned}\nu I_0 &= \nu \left(\int_P^Q \frac{\partial \psi_{0B}}{\partial x} dy - \int_Q^R \frac{\partial \psi_{0A}}{\partial y} dx + \int_R^S \frac{\partial \psi_{0B'}}{\partial x} dy - \int_S^P \frac{\partial \psi_{0A'}}{\partial y} dx \right) \\ &= \nu (I_{0B} + I_{0A} + I_{0B'} + I_{0A'}).\end{aligned}\quad (\text{A.7})$$

Using equations (A.3) and (A.4), we obtain

$$\nu I_{0A} = -\frac{\nu L_x l_x}{2\beta} \frac{\partial^2 \tau^x(y_2)}{\partial y^2} - (L_x - l_x) \left(\frac{\alpha l_x}{\pi} \right)^{1/2} \frac{\partial \tau^x(y_2)}{\partial y}, \quad (\text{A.8})$$

$$\nu I_{0A'} = -\frac{\nu L_x (L_x - l_x)}{2\beta} \frac{\partial^2 \tau^x(y_1)}{\partial y^2} + l_x \left(\frac{\alpha (L_x - l_x)}{\pi} \right)^{1/2} \frac{\partial \tau^x(y_1)}{\partial y} \quad (\text{A.9})$$

Using equation (A.5), we obtain

$$\nu I_{0B} = \int_{y_1}^{y_2} \left[l_x \frac{\partial \tau^x}{\partial y} + \frac{L_x - l_x}{2} \frac{\partial \tau^x}{\partial y} \text{erfc}\left(-\frac{y - y_2}{w_1(0)}\right) \right] dy. \quad (\text{A.10})$$

Since there is a second term in the integrand originally for non-zero wind stress curl at $y = y_2$, we replace $\partial \tau^x(y)/\partial y$ with $\partial \tau^x(y_2)/\partial y$ (constant). Thus equation (A.10) becomes

$$\begin{aligned}\nu I_{0B} &= l_x [\tau^x(y_2) - \tau^x(y_1)] \\ &+ \frac{L_x - l_x}{2} \frac{\partial \tau^x(y_2)}{\partial y} \left\{ \delta \cdot \text{erfc}\left(\frac{\delta}{w_1(0)}\right) \right. \\ &\left. - 2 \left(\frac{\alpha l_x}{\pi} \right)^{1/2} \left[\exp\left(-\frac{\delta^2}{w_1(0)^2}\right) - 1 \right] \right\}.\end{aligned}\quad (\text{A.11})$$

Similarly,

$$\begin{aligned}\nu I_{0B'} &= (L_x - l_x) [\tau^x(y_1) - \tau^x(y_2)] \\ &- \frac{l_x}{2} \frac{\partial \tau^x(y_1)}{\partial y} \left\{ \delta \cdot \text{erfc}\left(\frac{\delta}{w_2(l_x)}\right) \right. \\ &\left. - 2 \left(\frac{\alpha (L_x - l_x)}{\pi} \right)^{1/2} \left[\exp\left(-\frac{\delta^2}{w_2(l_x)^2}\right) - 1 \right] \right\}.\end{aligned}\quad (\text{A.12})$$

The sum of the above equations gives equation (26). The last term in (A.8) is set off by the last term in (A.11). Also, the last term in (A.9) is set off by the last term in

(A.12). These cancellations originate because the friction on the western boundary currents becomes small due to broadening of the zonal jets. The discussion is the same as that in Subsection 3.1.

References

- Baker,D.J.,Jr.,1982. A note on Sverdrup balance in the Southern Ocean. *J.Mar.Res.*, 40(Suppl): 1-26.
- Deacon G.E.R.,1937. The hydrology of the Southern Ocean. *Discovery Rep.*, 15: 1-124.
- Gill,A.E.,1968. A linear model of the Antarctic Circumpolar Current. *J.Fluid Mech.*, 32: 465-488.
- Gill,A.E. and K.Bryan,1971. Effects of geometry on the circulation of a three-dimensional southern-hemisphere ocean model. *Deep-Sea Res.*, 18: 685-721.
- Godfrey,J.S.,1989. A Sverdrup model of the depth-integrated flow for the world ocean allowing for island circulation. *Geophys.Astrophys.Fluid Dynamics*, 45: 89-112.
- Hellerman,S. and M.Rosenstein,1983. Normal monthly wind stress over the world ocean with error estimates. *J.Phys.Oceanogr.*, 13: 1,093-1,104.
- Hidaka,K. and M.Tsuchiya,1953. On the Antarctic Circumpolar Current. *J.Mar.Res.*, 12: 214-222.
- Johnson,M.A.,1989. Forcing the volume transport through Drake Passage. *J.Geophys.Res.*, 94: 16,115-16,124.
- Klinck,J.M.,1986. Channel dynamics and its application to the Antarctic Circumpolar Current. In: J.J.O'Brien (Editor), *Advanced Physical Oceanography Numerical Modelling*. D.Reidel Publishing Company, pp.299-328.
- McWilliams,J.C.,W.R.Holland and J.H.S.Chow,1979. A description of numerical Antarctic Circumpolar Current. *Dyn.Atmos.Oceans.*, 2: 213-291.
- Minato and Kimura,1980. Volume transport of the western boundary current penetrating into a marginal sea. *J.Oceanogr.Soc.Japan*, 36: 185-195.
- Munk,W.H. and E.Palmen,1951. Note on the dynamics of the Antarctic Circumpolar Current. *Tellus*, 3: 53-55.

- Nowlin, W.D., Jr. and J.M. Klinck, 1986. The physics of the Antarctic Circumpolar Current. *Rev. Geophys.*, 24: 469-491.
- Peterson, R.G., 1988. On the transport of the Antarctic Circumpolar Current through Drake Passage and its relation to wind. *J. Geophys. Res.*, 93: 13,993-14,004.
- Peterson, R.G. and T. Whitworth III., 1989. The Subantarctic and Polar Fronts in relation to deep water masses through the Southwestern Atlantic. *J. Geophys. Res.*, 94: 10,817-10,838.
- Stommel, H., 1948. The westward intensification of wind-driven currents. *Trans. Amer. Geophys. Un.*, 29: 202-206.
- Stommel, H., 1957. A survey of ocean current theory. *Deep-Sea Res.*, 4: 149-184.
- Stommel, H., 1962. An analogy to the Antarctic Circumpolar Current. *J. Mar. Res.*, 20: 92-96.
- Treguier A.M. and J.C. McWilliams, 1989. Topographic influences on wind-driven, stratified flow in a β -plane channel: An idealized model for the Antarctic Circumpolar Current. *J. Phys. Oceanogr.*, 20: 321-343.
- Wearn, R.B. and D.J. Baker, Jr., 1980. Bottom pressure measurement across the Antarctic Circumpolar Current and their relation to the wind. *Deep-Sea Res.*, 27A: 875-888.
- Whitworth T., III., W.D. Nowlin and S.J. Worley, 1982. The net transport of the Antarctic Circumpolar Current through Drake Passage. *J. Phys. Oceanogr.*, 12: 960-971.
- Whitworth T., III., 1983. Monitoring the transport of the Antarctic Circumpolar Current at Drake Passage. *J. Phys. Oceanogr.*, 13: 2,045-2,057.
- Wolff, J.-O. and D.J. Olbers, 1989. The dynamical balance of the Antarctic Circumpolar Current studied with an eddy resolving quasi-geostrophic model. In: J.C.J. Nihoul and B.M. Jamart (Editors), *Mesoscale-Synoptic coherent Struc-*

tures in Geophysical turbulence. Elsevier, Amsterdam, pp. 435-458.

Wolff J.-O., E.Maier-Reimer and D.J.Olbers,1991. Wind-driven flow over topography in a zonal β -plane channel: A quasi-geostrophic model of the Antarctic Circumpolar Current. J.Phys.Oceanogr., 21: 236-264.

Captions:

Fig. 1. Bottom topography near Drake Passage with a contour interval of 1 km.

Depths less than 3 km are shaded.

Fig. 2. The geometry of the model.

Fig. 3. A schematic diagram of the boundary layers that exist when the friction coefficient ν is small.

Fig. 4. The path (PQRSP) of integration used to obtain the transport. The lines PQ, RS are along the eastern coasts of the meridional barriers. The discussion of the path PS'R'Q'P' is in Section 4.

Fig. 5. Transport as a function of the overlapping length δ . The thick line is the solution in the limiting case with no friction. The friction coefficient ν ranges from 10^{-7}s^{-1} (curve labeled a) to $5 \times 10^{-7}\text{s}^{-1}$ (curve labeled e). As ν increases, the transport decreases.

Fig. 6. Transport as a function of the distance l_x . The thick line is the solution in the limiting case with no friction. ν varies in the same way as in Fig. 5.

Fig. 7. Transport as a function of the latitude y_0 where the eastward wind stress is a maximum. The numbers 1, 2 and 3 correspond to NM_1, NM_2, NM_3 . The thick line shows the sum of the three terms, or the total transport.

Fig. 8. As in Fig. 7 except that ν varies in the same way as in Fig. 5.

Fig. 9. Transport lines with $y_0 = 2000\text{km}$ (a) and 3000km (b). The stream functions are normalized by the values of the transport through the channel. The values of the transport are 167Sv (a), and 119Sv (b). Shaded areas indicate anti-clockwise circulation.

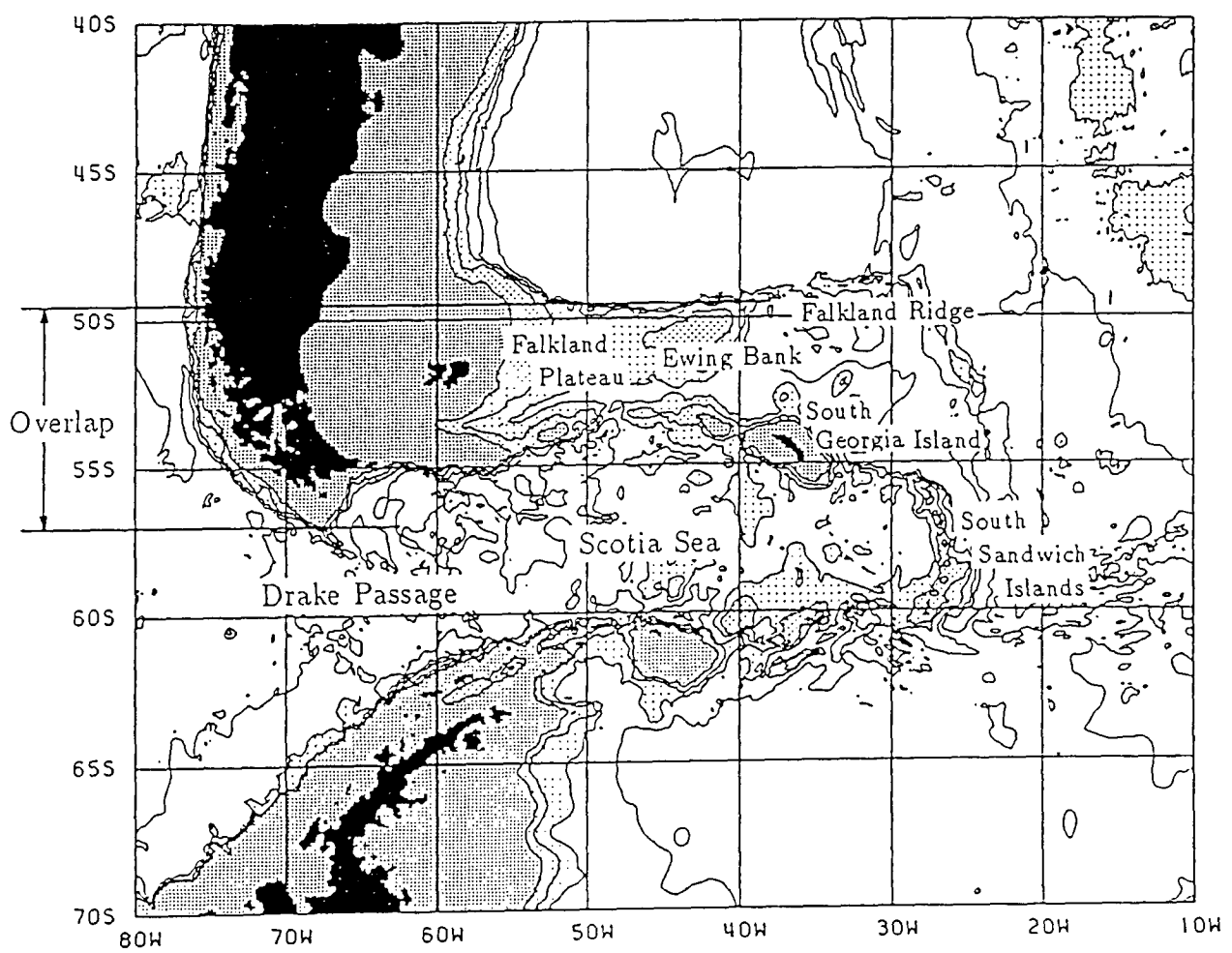


Fig. 1

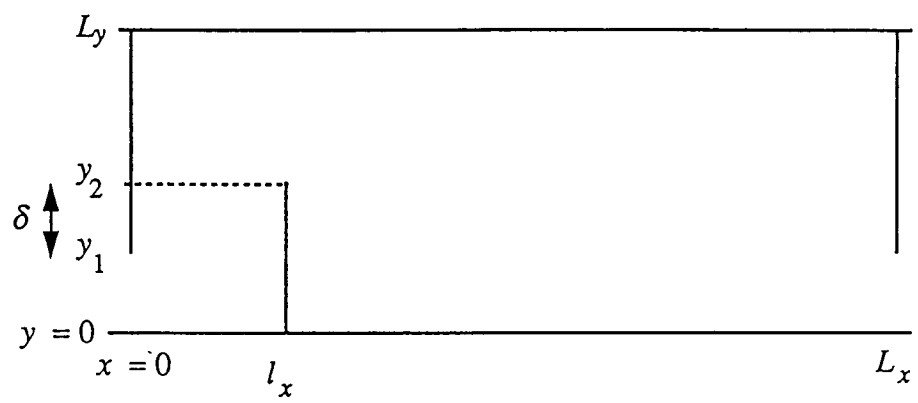


Fig. 2

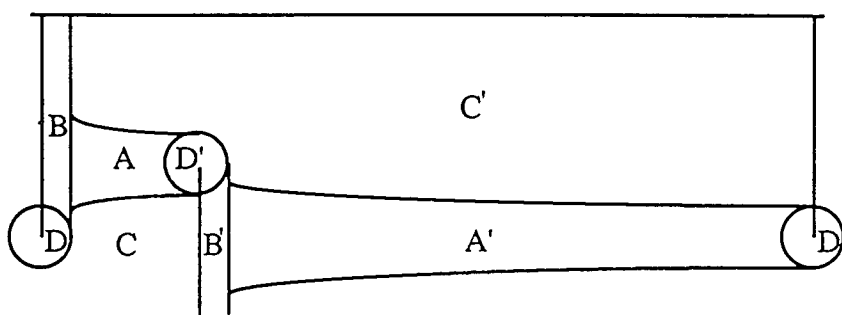


Fig. 3

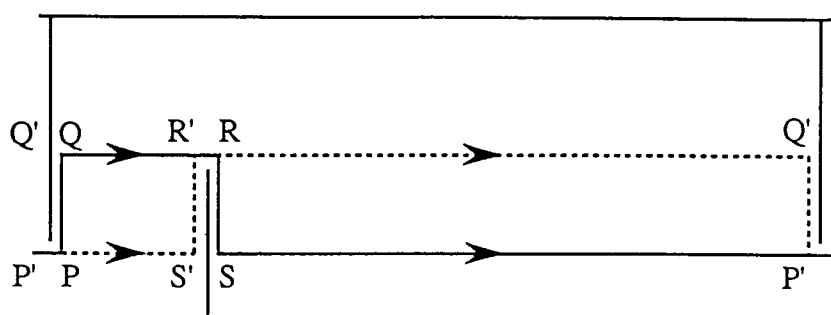


Fig. 4

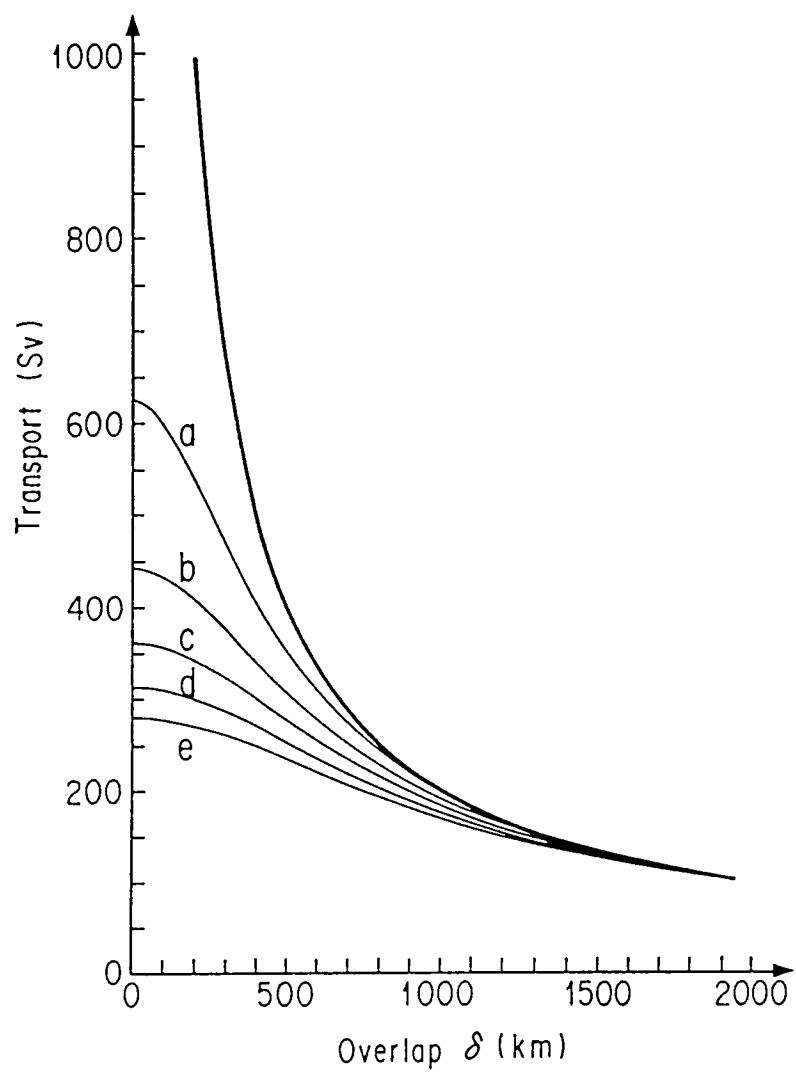


Fig. 5

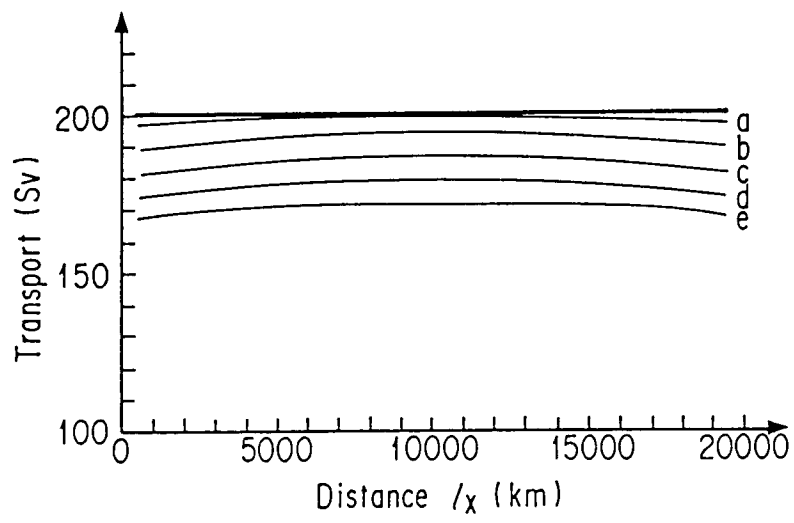


Fig. 6

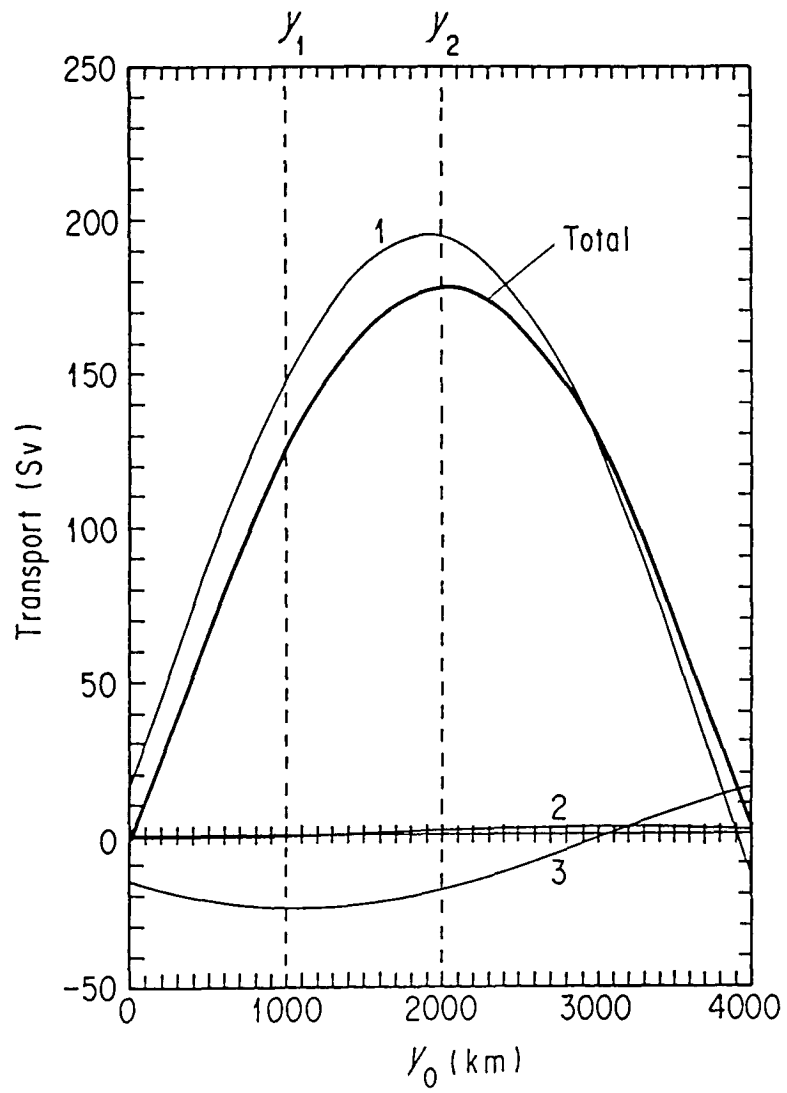


Fig. 7

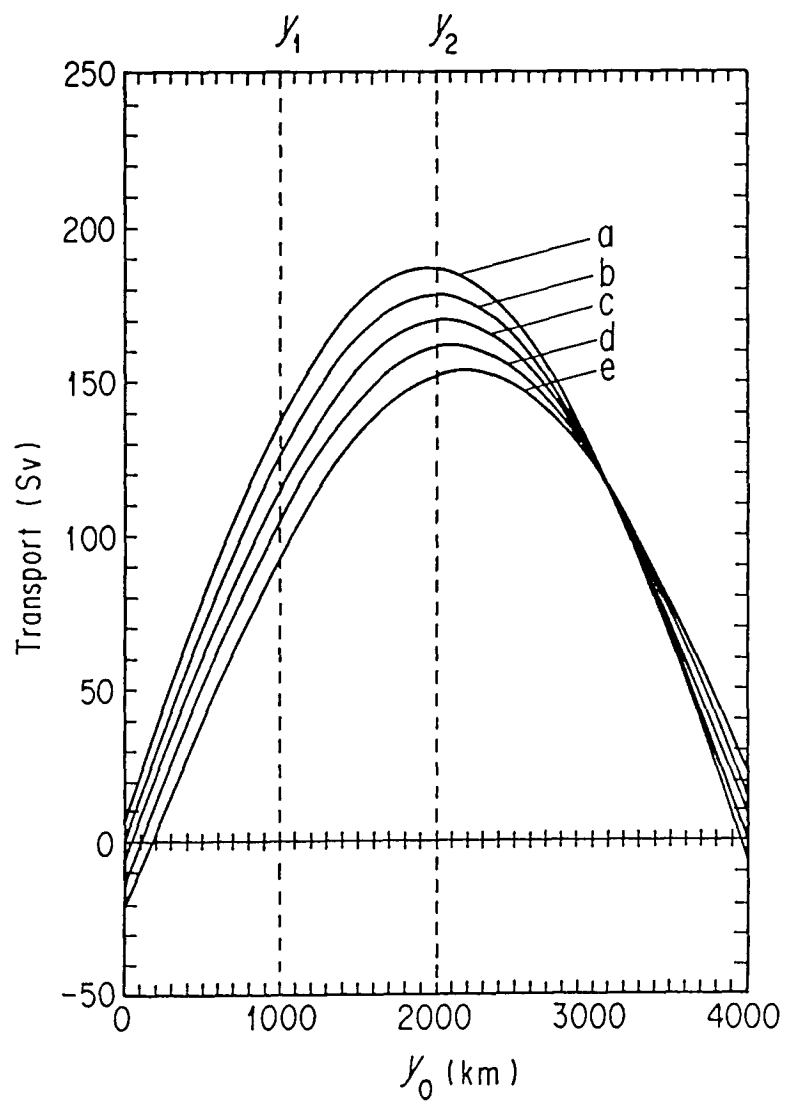


Fig. 8

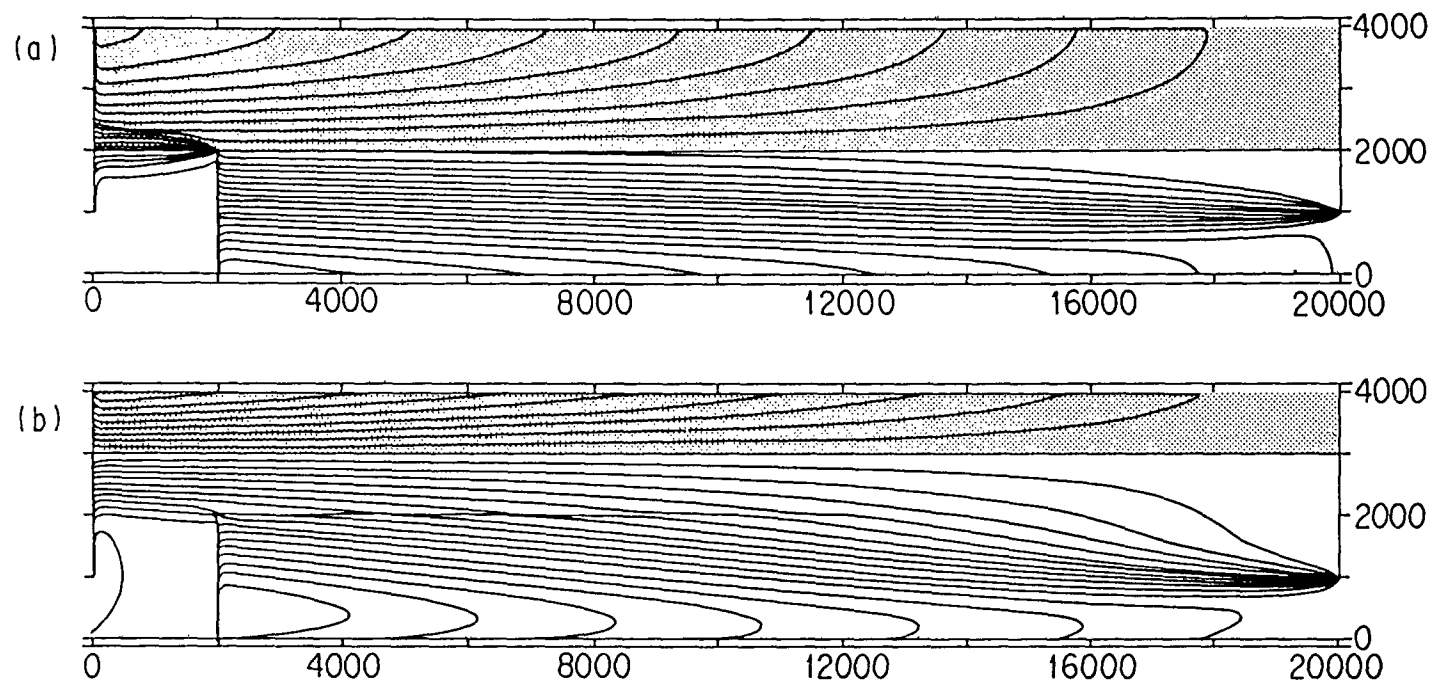


Fig 9

Effects of partial meridional barriers
on the Antarctic Circumpolar Current
– Buoyancy-driven three-layer model –

Akio Ishida

Abstract

The transport and vertical structure of the Antarctic Circumpolar Current (ACC) are examined, especially the component of the current driven by buoyancy, by using a three-layer model. We investigate the effects of the South American peninsula, the island arc to the east, and the Macquarie ridge, which are modeled as partial meridional barriers overlapping meridionally each other. We found that the buoyancy-driven component is given as a function of the transport out of the Weddell Sea (S_w) and the sum of the transports into the North Atlantic (S_A) and the North Pacific (S_P) out of the Southern Ocean. The buoyancy-driven current flows westward, if S_w and S_A+S_P are positive. The transport depends on the value of S_w more than S_A+S_P by one order of magnitude within a realistic range of parameters. The most predominant term in the transport equation is inversely proportional to the difference between the Coriolis parameters at the tips of the partial meridional barriers. Thus, the magnitude of the transport strongly depends on the overlapping length of the meridional barriers. The eastward current of the ACC is driven by the predominant eastward wind stress in the Southern Ocean, although a part of the wind-driven component is canceled by the westward buoyancy-driven component. The vertical structure of the ACC is found to be attributed to the surface wind-driven circulation and the deep and bottom buoyancy-driven circulation.

1. Introduction

The Southern Ocean, or Antarctic Ocean, is the only zonally unbounded region among the world oceans. The Antarctic Circumpolar Current (ACC) flows eastward in the region and carries abyssal water to the world oceans. Thus, it is important to investigate the volume transport and the structure of the ACC to understand the global ocean circulation and water formation.

To date, the ACC has been studied as a wind-driven ocean current by using barotropic models (Munk and Palmén, 1951; Hidaka and Tsuchiya, 1953; Gill, 1968; Johnson and Hill, 1975; Baker, 1982; Klinck, 1986). Hidaka and Tsuchiya (1953) constructed models of the ACC as a laterally viscous zonal stream driven by surface wind stress. To limit the total transport of the ACC within the observed values, a lateral eddy viscosity of more than $10^{10} \text{ cm}^2 \text{ s}^{-1}$ was required by their models – several orders of magnitude greater than that generally envisaged in other oceanic currents. Many efforts have been made to find a dynamical balance for the ACC that allows for observed surface wind stress as a driving force while maintaining reasonable transport values.

Ishida (1994) investigated the effects of the South American peninsula and the island arc to the east of Drake Passage on the ACC using a barotropic model. The South American peninsula and the island arc were modeled as two partial meridional barriers overlapping each other in a latitude band. The transport of the ACC was given by the magnitude of the zonal wind stress at the latitudes of the ends of two meridional barriers and the difference between the Coriolis parameters at the same latitudes. The topographic drag on the meridional barriers was shown as the force balancing the surface wind stress. The transport value predicted by Ishida's model was reasonably compared with observed values. This suggests that the existence of the meridional barriers overlapping each other in a latitude band plays an important

role in the transport and structure of the ACC.

While research on the ACC as a wind-driven circulation is ongoing, the buoyancy effects on the ACC and the coupled wind- and buoyancy-driven circulation have not yet been investigated. Some observations and data analysis (Rintoul, 1991; Whitworth *et al.*, 1991) have suggested the importance of buoyancy effects on the circulation in the Southern Ocean.

Rintoul (1991) estimated the exchange of water mass between the South Atlantic poleward of 32° S and the neighboring ocean basins using hydrographic data and inverse methods. There was the westward flow near the bottom in the northern portion of Drake Passage. The velocity field across Drake Passage is similar to that obtained by Nowlin *et al.* (1977) (see their Figure 11), who used short-term current meter measurements to reference geostrophic calculations based on the same hydrography used by Rintoul (1991). The westward flow in the bottom layer is suggested to be driven by buoyancy rather than the wind stress, because the predominant wind over the Southern Ocean is eastward.

Whitworth *et al.* (1991) showed that a current flows westward along the northern flank of the Falkland Plateau from bottom to at least 1000 m. The mean transport was 8.2 Sv (1 Sv = $10^{12} \text{ cm}^3 \text{ s}^{-1}$) to the west with variability induced by the meandering of the overlying ACC. They suggested that the westward flow was similar to the boundary current along the southern boundary in a closed basin predicted by Stommel and Arons (1960a). However, application of the Stommel-Arons theory is not straightforward when applied to zonally periodic basins such as is found in the Southern Ocean. The bottom westward currents through Drake Passage and along the northern flank of the Falkland Plateau may be portions of the zonal recirculation in the Southern Ocean rather than locally driven currents, and the pronounced topographies, such as the South American peninsula and the Falkland Plateau, are expected to play an important part in recirculation.

The buoyancy effects on the ACC have been investigated in global abyssal circulation models. Stommel (1958) showed a schematic pattern of global abyssal circulation with two sources of abyssal water in the North Atlantic and the Weddell Sea. The abyssal water from the North Atlantic, together with that from the Weddell Sea, flows eastward in the Southern Ocean, and then extends up northward into the Indian and Pacific Oceans. Although the abyssal currents in the Southern Ocean were depicted to be eastward currents in the figure, the direction and transport of the currents were not determined based on a dynamical theory, as stated in his paper.

Stommel and Arons (1960b) derived a schematic budget of transports in various portions of the World Ocean. An arbitrary value was assigned to the transport around the Antarctic Continent in the budget because they did not have an adequate understanding of just what happens dynamically in this region.

Kuo and Veronis (1973) and Kuo (1978) attempted to study the abyssal oxygen distribution using the model by Stommel and Arons (1960a). The recirculation transport around the Antarctic Continent was prescribed as a parameter because of the reason stated above. They showed that a best fit to the observed oxygen was given, if the recirculation was fixed at 35Sv.

As stated above, no model that can has yet described the buoyancy-driven circulation in a zonally unbounded basin such as the Southern Ocean based on dynamically consistent discussion. The main objective of this paper is to describe the effects of partial meridional barriers on the ACC mainly with regard to buoyancy-driven circulation. The problem to be considered, then, is how the buoyancy-driven circulation is described in a zonally unbounded basin such as the Southern Ocean. Buoyancy effects are included as exchange of fluids between the layers. The zonal transport of the buoyancy-driven recirculation can be predicted

in the model basin similar to that of Ishida (1994), which includes the meridional barriers overlapping each other. We also discuss the vertical structure of the ACC, including wind stress effects in the model in section 5. While bottom bathymetry is not included in the model basin of this study, such a model should be constructed to realistically describe the ACC. The main objective of this paper is to illustrate how partial meridional barriers affect the buoyancy-driven component of the transport of the ACC. Therefore, we only studied the effects of lateral topography.

2. Model formulation

The model used in this study is a three-layer model, as depicted in Fig. 1. The uppermost layer corresponds the surface and intermediate layers. The middle layer corresponds the deep layer occupied by the North Atlantic Deep Water (NADW) and the lowest layer corresponds the bottom layer occupied by the Antarctic Bottom Water. The mean thickness of each layer is H_k , and the interfacial deviation from rest state is η_k . The density in each layer is represented as ρ_k . The subscript k indicates that the symbol corresponds to the k th layer.

The buoyancy effects are incorporated as exchange of fluids between the layers. The rate (w_{ij}) of exchange between layer i and layer j is specified as a spatially constant value. Tziperman (1986) and Kawase (1987) suggest that the upwelling velocity is a function of the layer height field. In this study, for simplicity, and because our primary interest is how buoyancy affects the circulation in the Southern Ocean, we specify w_{ij} to be spatially constant. Since the buoyancy driven circulation is focused in this study, the surface wind stress is not included in the model except in section 5.

The model geometry used in this study is depicted in Fig. 2. A spherical coordinate system is used where λ represents longitude, φ represents latitude, and r is the radius of the

earth. The model is of the Southern hemisphere basin with three meridional barriers. The whole basin is divided into subregions I to V. The lines $\varphi = 0$ and $\varphi = \varphi_0$ represent the equator and the Antarctic coastline, respectively. The lines $\lambda = 0$ and $\lambda = \lambda_0$ represent the same meridian, the section $\varphi_1 < \varphi < 0$ being a barrier similar to the South American peninsula. The line $\lambda = \lambda_1$ represents the second meridional barrier, which corresponds to the island arc formed by the South Sandwich and South Shetland islands.

Stommel (1957) modeled the South American peninsula and the island arc as two partial meridional barriers. He emphasized that the ACC cannot be purely zonal because there is no latitude band without a meridional barrier. Thus the southern end of the South American peninsula and the northern end of the island arc were settled on the same latitude in his model. However, if we regard the island arc, the Ewing Bank and the Falkland ridge, as the second meridional barrier, the South American peninsula and the second barrier overlap in latitude. So the northern end of the second meridional barrier at $\lambda = \lambda_1$ is settled to the north of the southern end of the first barrier at $\lambda = 0$. The line $\lambda = \lambda_2$ represents the third meridional barrier, which corresponds to the boundary between the Indian and Pacific Oceans. The southern part of this barrier represents the Macquarie ridge, and the southern end is settled at the same latitude as the southern end latitude of the South American peninsula for simplicity. The boundary between the Atlantic and the Indian Ocean is not included in the model because the boundary does not affect the circulation in the Southern Ocean. This is because the southern end of the African Continent is north of the latitude φ_2 .

The basin geometry is similar to that of Ishida (1994), but the meridional barrier at $\lambda = \lambda_2$ is added to find the effects of outflow of deep water to the North Pacific. The difference between the results in Ishida (1994) and in this study due to inclusion of the barrier at $\lambda = \lambda_2$ is discussed in section 5.

The net upward flux out of layer equals the net inflow flux from the neighboring basins. The inflow flux from the Weddell Sea is S_{wk} , and the outflow flux to the North Atlantic and the North Pacific across the equator are S_{Ak} , S_{Pk} , respectively. The subscript k indicates that the symbol corresponds to the k th layer. For mass conservation, the following relation is given,

$$-w_k r^2 \lambda_0 \sin \varphi_0 = S_{wk} - (S_{Ak} + S_{Pk}), \quad (1)$$

where w_k is the net upward outflow out of the k th layer, that is given by

$$w_k = \begin{cases} -w_{12} & : k = 1 \\ w_{12} - w_{23} & : k = 2 \\ w_{23} & : k = 3 \end{cases} \quad (2)$$

Each layer is assumed to be in geostrophic balance. The corresponding equations of motion and continuity in the k th layer are

$$-f v_k = -\frac{1}{\rho_0 r \cos \varphi} \frac{\partial p_k}{\partial \lambda}, \quad (3a)$$

$$f u_k = -\frac{1}{\rho_0 r} \frac{\partial p_k}{\partial \varphi}, \quad (3b)$$

$$\frac{\partial H_k u_k}{\partial \lambda} + \frac{\partial}{\partial \varphi} (H_k v_k \cos \varphi) = -w_k r \cos \varphi, \quad (3c)$$

where u and v are the eastward and the northward components of velocity, $f = 2\Omega \sin \varphi$ is the Coriolis parameter, Ω is the rate of planetary rotation, and p_k is the pressure given by;

$$p_k = \sum_{n=1}^k g_n \eta_n, \quad (4)$$

where g_n is the gravity acceleration or the reduced gravity given by ;

$$g_n = \begin{cases} g & : n = 1 \\ (\rho_2 - \rho_1) g / \rho_0 & : n = 2 \\ (\rho_3 - \rho_2) g / \rho_0 & : n = 3 \end{cases} \quad (5)$$

where g is the gravity acceleration and ρ_0 is the mean density. The interfacial deviation η_n is derived from p_k by using equation (4).

Because the above equations are similar to those used in Stommel and Arons (1960a), the same circulation as that shown in Stommel and Arons (1960a) is expected to be derived in an interior region. The difference between the present model and the Stommel-Arons model is that the model basin used in this study is zonally unbounded. Therefore, the zonal boundary currents are generated at the end latitudes of the meridional barriers. The boundary currents derived in this model correspond to the ACC. The boundary currents have the transports Q_{Ak} , Q_{Bk} , and Q_{Ck} as shown in Fig. 2.

The meridional transport in an interior region is found from the vorticity equation and the continuity equation (3c). It is given by

$$H_k v_k = w_k r \tan \varphi \quad (6)$$

Elimination of $H_k v_k$ from (3c) and (6) leads to the zonal transport given by

$$H_k u_k = -2w_k r (\lambda - \lambda_e) \cos \varphi. \quad (7)$$

where λ_e is a longitude at an eastern boundary. Elimination of v_k from (3a) and (6), and zonal integration of the derived equation lead to the pressure field given by

$$p_k = \frac{w_k}{H_k} \rho_0 f r^2 (\lambda - \lambda_e) \sin \varphi + p_{(e)k}, \quad (8)$$

where $p_{(e)k}$ is the value of p_k at $\lambda = \lambda_e$. The pressure $p_{(e)k}$ is usually set to zero because the

circulation in a closed basin is independent of the value. However, we must derive the values of pressure at the eastern boundaries in the model basin with multiple meridional barriers, and their derivation is represented in the next section.

The interior circulation in k th layer depends solely on the vertical flux w_k except the parameters of the basin geometry ($\lambda_1, \lambda_2, \lambda_0, \varphi_1, \varphi_2, \varphi_0$). Thus we can investigate the circulation in each layer independently, if the flux w_k or the net inflow $S_{wk} - (S_{Ak} + S_{Pk})$ is specified.

There is no flow in interior regions, if the net upward flux is zero ($w_k = 0$). However, the transports Q_{Ak} , Q_{Bk} , and Q_{Ck} of the zonal boundary currents are not necessarily zero, because they depend on the magnitude of the flux from the neighboring basins. The dependence on flux is investigated in the next section.

3. Solution

The purpose of this section is to derive the transport of the zonal current and the values of pressure at the eastern boundaries in the model basin. We show how the buoyancy-driven circulation is determined in a zonally unbounded basin. The subscript k is omitted in this section because the solution is derived in the k th layer.

We set the eastern boundary values of pressure as follows: Zero at the eastern boundary of regions II and IV, $p_{(4l)}$ at that of regions I and III, $p_{(2l)}$ at that of region V. The value of pressure at the eastern boundary of regions II and IV is arbitrary because the transport of the zonal boundary current depends on the deviation of pressure, but not on the pressure itself. The meridional pressure difference across the line $\varphi = \varphi_2$, $0 < \lambda < \lambda_1$ can be represented with $p_{(4l)}$, after the interior pressure is given by (8). Using equations (3b) and (8), we can obtain the relation equation between Q_A and $p_{(4l)}$;

$$Q_A = w r^2 (\lambda_2 - \lambda_1) \sin \varphi_2 - H p_{(e1)} / f_2 , \quad (9a)$$

where f_2 is the Coriolis parameter at the latitude φ_2 . In the same way, the relations between Q_B and $p_{(e1)}$ and between Q_C and $p_{(e2)}$ are given by

$$Q_B = -w r^2 (\lambda_0 + \lambda_1 - \lambda_2) \sin \varphi_1 - H p_{(e1)} / f_1 , \quad (9b)$$

$$Q_C = -w r^2 \lambda_1 \sin \varphi_1 - H p_{(e2)} / f_1 , \quad (9c)$$

where f_1 is the Coriolis parameter at latitude φ_1

Consider the mass exchange between region III and the other neighboring regions. The total inward flux of mass to region III consists of some parts: the flux of the western boundary current across $\varphi = \varphi_1$ at $\lambda = \lambda_1$, the net vertical flux integrated over the area, the net meridional flux across φ_1 and φ_2 in the interior of the ocean, The net influx of the zonal currents on $\varphi = \varphi_1$ and φ_2 . Since the sum of these components must be zero because of the mass conservation, we can get the following equation,

$$Q_A - Q_B = -(S_A - S_P) + 2w r^2 [(\lambda_0 + \lambda_1 - \lambda_2) \sin \varphi_1 + (\lambda_2 - \lambda_1) \sin \varphi_2] \quad (10a)$$

This equation gives the relation between Q_A and Q_B . Since the difference between Q_B and Q_C equals the northward transport of the western boundary current from region IV' to region V. the equation is given by

$$Q_B - Q_C = S_P - 2w r^2 (\lambda_0 - \lambda_2) \sin \varphi_1 \quad (10b)$$

Now there are five equations (9a,b,c) and (10a, b) and five unknowns (Q_A , Q_B and Q_C , $p_{(e1)}$, $p_{(e2)}$). The transport of the zonal currents and the pressure at the eastern boundaries are derived as follows:

$$Q_A = w r^2 (\lambda_2 - \lambda_1) \sin \varphi_2 + f_1 S_x / (f_2 - f_1), \quad (11a)$$

$$Q_B = -w r^2 (\lambda_0 + \lambda_1 - \lambda_2) \sin \varphi_1 + f_2 S_x / (f_2 - f_1), \quad (11b)$$

$$Q_C + S_P = w r^2 (\lambda_0 - \lambda_1 - \lambda_2) \sin \varphi_1 + f_2 S_x / (f_2 - f_1), \quad (11c)$$

$$Hp_{(e1)} = -f_1 f_2 S_x / (f_2 - f_1), \quad (12a)$$

$$Hp_{(e2)} = Hp_{(e1)} + f_1 [S_P - w r^2 (\lambda_0 - \lambda_2) \sin \varphi_1], \quad (12b)$$

where S_x is given by

$$S_x = (S_A + S_P) \frac{\lambda_0 (\sin \varphi_0 - \sin \varphi_1) + (\lambda_2 - \lambda_1) (\sin \varphi_1 - \sin \varphi_2)}{\lambda_0 \sin \varphi_0} + S_W \frac{(\lambda_0 + \lambda_1 - \lambda_2) \sin \varphi_1 + (\lambda_2 - \lambda_1) \sin \varphi_2}{\lambda_0 \sin \varphi_0} \quad (13)$$

The transports Q_A , Q_B and Q_C are given as functions of the transports S_w , S_A , and S_P . However, the transports Q_A , Q_B , and $Q_C + S_P$ can be represented as functions of the transports S_w and $S_A + S_P$, as shown in (11a,b,c). Thus, we may investigate the dependence of the zonal current transports to S_w and $S_A + S_P$.

Equations (11a,b,c) include the terms inversely proportional to $f_2 - f_1$. Since the magnitude of $f_2 - f_1$ in the denominator is smaller than f_1 or f_2 in the numerator by one order, the terms are predominant in the equations. The dependence of the transports Q_A , Q_B , and Q_C on the model basin geometry is essentially determined by the dependence of the term S_x on the geometry because the term including S_x predominates in (11a,b,c). Equation (13) is rewritten to

$$S_x = (S_A + S_P) \cdot (\text{Area of Region III, IV, IV'}) / (\text{Total area of model basins}) + S_w \cdot (\text{Area of Region I, II, V}) / (\text{Total area of model basins}) \quad (14)$$

Regions III, IV, and IV' are the polar regions from about the latitude band, which the

meridional barriers overlap, and regions I, II, and V are the equatorial regions. Thus the ratio of the area in R.H.S. of (14) depends on latitude φ_1 and φ_2 . It is expected that S_x depends on S_w more than $S_A + S_p$ because the area of the equatorial regions is larger than that of the polar regions. Since the coefficient of S_x is inversely proportional to $f_2 - f_1$, it is expected that the transport of the zonal currents strongly depends on φ_2 and φ_1 . If a rough estimation of parameters is given as follows: $\varphi_0 = 70^\circ\text{S}$, $\varphi_1 = 60^\circ\text{S}$, $\varphi_2 = 50^\circ\text{S}$, $\lambda_0 = 360^\circ$, $\lambda_1 = 30^\circ$, $\lambda_2 = 180^\circ$, S_x is given by

$$S_x = 0.12 (S_A + S_p) + 0.88 S_w.$$

Thus we find that S_x depends on S_w more than $S_A + S_p$ and the zonal current transport also depends on S_w .

The physical interpretation of S_x can be obtained by investigating the solution of the simplified situation where vertical flux is zero ($w=0$), as described below. The zonal currents and the interior circulation are driven by buoyancy, which is incorporated as the net inward flux $S_w - (S_A + S_p)$ from the other basins and as the exchange of fluids between the layers in this study. If the net inward flux from the other basins is zero (if exchange between the layers is zero), there is no circulation in the interior regions. However, as seen from equations (11a,b,c), the zonal current transport is not zero even if exchange between the layers is zero. For example, the transports of zonal currents are $Q_A = f_1 S / (f_2 - f_1)$ and $Q_B = Q_C = f_2 S / (f_2 - f_1)$ under the condition that inflow S out of the Weddell Sea and outflow S into the North Atlantic ($S_w = S_A = S$, $S_p = 0$). These are derived from (11), and S_x equals S as found by (13). The westward currents are generated because of the high pressure in the southern side of the basin owing to the inflow out of the southern boundary. The magnitude of the transport is provided when the resistance on the western boundary currents balances the driving force.

These solutions can also be derived by the discussion described in Section 4 of Ishida (1994). If Drake Passage is presumed to be closed by a meridional barrier, the water out of the Weddell Sea flows northward along the eastern boundary of the meridional barrier at $\lambda=\lambda_1$, and turns west at latitude φ_2 as a zonal boundary current, and flows northward again along the barrier at $\lambda=0$. The pressure difference across the barrier is caused by these boundary currents. The pressure difference is given by $f_2 S/H$ when the transport out of the Weddell Sea is S . This is obtained under the assumption of geostrophic balance to the zonal currents on the line $0 < \lambda < \lambda_1$, $\varphi = \varphi_2$. If the barrier is removed, recirculation around the Antarctic Continent is generated. The transport is provided when the pressure difference balances the pressure decrease along the recirculation caused by the resistance. The pressure decrease along the recirculation is $(f_2 - f_1)Q/H$ if the transport of the recirculation is Q . Then, the transports of the zonal currents are given as follows: $Q_A = f_1 S / (f_2 - f_1)$, $Q_B = Q_C = f_2 S / (f_2 - f_1)$.

Thus, we found that transport of the buoyancy-driven zonal current can be derived according to the discussion in Ishida (1994), who showed that the driving force of the wind-driven zonal current was given by the pressure difference at Drake Passage. Transport S_* is part of the driving force of the buoyancy-driven recirculation, and is $Q_B - Q_A$ when $w = 0$.

Figure 3a shows a schematic view of the boundary currents derived above. Similarly, schematic views of the circulation driven by flux S out of the Weddell Sea into the North Pacific (Fig. 3b) and out of the North Atlantic into the North Pacific (Fig. 3c) are also drawn. The transports of the zonal currents in Fig. 3b are the same as in Fig. 3a except $Q_C = f_1 S / (f_2 - f_1)$. In the situation where the Weddell Sea is not included as source or sink (Fig. 3c), Q_A and Q_B are zero, and the transport Q_C is equal to inflow flux S .

The direction of the zonal current is determined by the positions of source and sink. Zonal current is westward (eastward) when flow is from (into) the Weddell Sea (Fig. 3a, b). Zonal

current is westward (eastward) when flow is from (into) the North Atlantic and into (from) the North Pacific (Fig. 3c). The component driven by exchange between the layers must be added in the real ocean. The relation between the total transport of the zonal currents and the fluxes out of the source and into the sink is described in the next section.

4. Parameter sensitivities

Now we examine the parameter sensitivities of the solutions derived in the previous section. The transports Q_A , Q_B , and Q_C+S_P are proportional to the transports S_W and S_A+S_P , and are given by

$$\begin{pmatrix} Q_A \\ Q_B \\ Q_C + S_P \end{pmatrix} = \begin{pmatrix} p_A \\ p_B \\ p_C \end{pmatrix} S_W + \begin{pmatrix} q_A \\ q_B \\ q_C \end{pmatrix} (S_A + S_P). \quad (15)$$

Thus, the dependence of the proportional coefficients (p_A , p_B , p_C , q_A , q_B , q_C) on the model basin geometry were investigated to study the parameter sensitivities of the zonal current transports. In particular, we show the dependence on the positions of the tips of the meridional barriers (φ_1 and φ_2) because the transports depend on φ_1 and φ_2 more than the other parameters.

Figure 4 shows the proportional coefficients (p_A , p_B , and p_C) as functions of the latitudes φ_1 and φ_2 . The values shown in the figure equal the transport of the zonal current when $S_W=1$, $S_A+S_P=0$. Latitude φ_1 represents the southern end of the South American peninsula and is about 57° S. Latitude φ_2 represents the northern end of the island arc to the east of Drake Passage and is about 53° S, if the northern tip of the South Georgia Island is chosen as φ_2 . However, if we regard the island arc, the Ewing Bank, and the Falkland ridge as the second meridional barrier, as described in section 2, the northern end of the barrier is to the north of

latitude 50°S . Thus, the range of φ_2 in Fig. 4 is set north of latitude 50°S . The parameters except φ_1 and φ_2 are as follows: $\varphi_0 = 70^\circ\text{S}$, $\lambda_1 = 30^\circ$, $\lambda_2 = 180^\circ$, $\lambda_0 = 360^\circ$.

All the values in Fig. 4 are negative, and the result shows that westward currents are driven by the inward flux from the Weddell Sea. Since Figure 4(c) shows the transport $Q_C + S_p$, the zonal current in the Pacific sector is not necessarily westward. However, since deep water is thought to be supplied into the North Pacific ($S_p > 0$), the westward current is probably driven by the inflow out of the Weddell Sea in deep Pacific as well.

The magnitude of the zonal current transport increases as $\sin\varphi_2 - \sin\varphi_1$ decreases, as stated in the previous section. Figure 4 shows that the magnitude increases from the position $\varphi_1 = 60^\circ\text{S}$ and $\varphi_2 = 45^\circ\text{S}$ to the position $\varphi_1 = 55^\circ\text{S}$ and $\varphi_2 = 50^\circ\text{S}$. The values of p_A , p_B , and p_C are about from -4 to -12 in the range of φ_1 and φ_2 (Fig. 4).

Figure 5 shows the proportional coefficients (q_A , q_B , and q_C) as functions of latitudes φ_1 and φ_2 . The values shown in the figure equal the transport of zonal current when $S_w=0$, $S_A+S_p=1$. The results in Fig. 5 show the same tendency as Fig. 4 at points where the value is negative, and the magnitude of the zonal current transport increases as $\sin\varphi_2 - \sin\varphi_1$ decreases. However, the magnitude of p_A , p_B , and p_C is larger than that of q_A , q_B , and q_C , which is in the range -0.4 to -2.5 . This shows that the magnitude of the zonal current transport driven by S_w is larger than that driven by S_A+S_p . As described in the discussion about Eq. (14), this is because the area of equatorial regions of the overlapping latitude band is larger than that of polar regions.

Another difference of the results in Fig. 4 and Fig. 5 is the manner of the dependence on φ_1 and φ_2 . If φ_1 and φ_2 are set more to the equatorial side keeping $\varphi_2 - \varphi_1$ at a certain value (from the point $\varphi_1 = 60^\circ\text{S}$ and $\varphi_2 = 50^\circ\text{S}$ to the point $\varphi_1 = 55^\circ\text{S}$ and $\varphi_2 = 45^\circ\text{S}$), the magnitude of the transport driven only by the the flux from the Weddell Sea decreases (Fig. 4).

However, the magnitude of the transport driven by the flux into the Northern hemisphere increases (Fig. 5) because factor S_* increases as found in (14). The zonal current transport becomes more sensitive to the magnitude of the flow out of the Weddell Sea (the Northern hemisphere) as the latitude band that the meridional barriers overlap is set to poleward (equatorward). However, the sensitivity to the position of the latitude band is less than that to the magnitude of $\varphi_2 - \varphi_1$, and the range of the magnitude of the transport is at most 1.5 in Fig. 4 and 0.3 in Fig. 5.

5. Wind stress effects on the Circulation

Now we examine the effects of wind stress on the zonal current transport and the interior circulation. If surface wind stress is added to the equations (3a, b, c) and the upward fluxes introduced to express buoyancy effects are omitted, the equations (3a, b, c) become

$$-f v_k = -\frac{1}{\rho_0 r \cos \varphi} \frac{\partial p_k}{\partial \lambda} + \tau^\lambda, \quad (16a)$$

$$f u_k = -\frac{1}{\rho_0 r} \frac{\partial p_k}{\partial \varphi}, \quad (16b)$$

$$\frac{\partial H_k u_k}{\partial \lambda} + \frac{\partial}{\partial \varphi} (H_k v_k \cos \varphi) = 0, \quad (16c)$$

where τ^λ is eastward wind stress which acts only on the uppermost layer. The meridional component of the wind stress is neglected because it is smaller than the zonal component. The wind stress distribution is assumed to be zonally uniform for simplicity. The assumption of no stress-transfer across the interfaces, so that the middle and lowest layers are quiescent, is equivalent to assuming zero horizontal pressure gradients in the lower layers. We thus focus on the circulation in the top layer and omit subscript k in the following equations.

Elimination of pressure by cross differentiating (16a) and (16b) and use of (16c) yield the Sverdrup meridional transport relation

$$\beta H v = -\frac{1}{r \cos \varphi} \frac{\partial}{\partial \varphi} (\tau^\lambda \cos \varphi), \quad (17)$$

where $\beta = -\frac{1}{r} \frac{df}{d\varphi}$

We integrate (16a) zonally to obtain

$$p = \rho_0 r \cos \varphi [f H v + \tau^\lambda] (\lambda - \lambda_e) / H + p_e, \quad (18)$$

where p_e is the value of pressure at $\lambda = \lambda_e$, a longitude near the eastern boundary. We can also obtain the zonal transport in the interior by substituting the value of $H v$ given by (17) to (16c) and integrating (16c) zonally.

The total zonal transports Q_A , Q_B , and Q_C driven by wind stress are given by the sum of the component of the recirculation Q around the Antarctic Continent and the component originated from the wind stress curl is not zero at latitudes φ_1 or φ_2 . For example, transport Q_A is given as the following. If the wind stress curl is not zero at latitude φ_2 , there is meridional flux given by (17) in the interior across the line $\varphi = \varphi_2$, $\lambda_1 < \lambda < \lambda_2$. Since the exchange of fluids between regions I and III must be zero, except for the net recirculation transport Q , the interior meridional flux across the line must be compensated for the supply of water by the zonal current on the line $\varphi = \varphi_2$, $0 < \lambda < \lambda_1$. The transport is $H v(\varphi_2) r (\lambda_2 - \lambda_1) \cos \varphi_2$, which is the value of the zonal integration of $H v$ at φ_2 given by (17). Thus, the transport Q_A is given by

$$Q_A = Q + H v(\varphi_2) r (\lambda_2 - \lambda_1) \cos \varphi_2. \quad (19a)$$

The transports Q_B and Q_C are given in the same way as follows:

$$Q_B = Q - H\nu(\varphi_1) r (\lambda_1 + \lambda_0 - \lambda_2) \cos \varphi_1, \quad (19b)$$

$$Q_C = Q - H\nu(\varphi_1) r \lambda_1 \cos \varphi_1. \quad (19c)$$

If the zonal currents at latitudes φ_1 and φ_2 are assumed to be in geostrophic balance, the transports Q_A , Q_B , and Q_C , given by (19a, b, c), are expressed with pressure differences across the zonal currents, i.e. the differences at the northern and southern side of the currents. If we set the eastern boundary values of pressures in the same way as in section 3, the geostrophic relations give the following equations:

$$f_2 Q = \tau^\lambda(\varphi_2) r (\lambda_2 - \lambda_1) \cos \varphi_2 - p_{(e1)}/\rho_0, \quad (20a)$$

$$f_1 Q = -\tau^\lambda(\varphi_1) r (\lambda_0 + \lambda_1 - \lambda_2) \cos \varphi_1 - p_{(e1)}/\rho_0, \quad (20b)$$

$$f_1 Q = -\tau^\lambda(\varphi_1) r \lambda_1 \cos \varphi_1 - p_{(e2)}/\rho_0. \quad (20c)$$

We can derive the net recirculation transport Q from these equations (20a, b, c): i.e.,

$$Q = [\tau^\lambda(\varphi_1) r (\lambda_0 + \lambda_1 - \lambda_2) \cos \varphi_1 + \tau^\lambda(\varphi_2) r (\lambda_2 - \lambda_1) \cos \varphi_2] / (f_2 - f_1). \quad (21)$$

This equation shows that the transport Q is given by the ratio of the line integrals of the zonal wind stress to the difference between the Coriolis parameters at the latitudes φ_2 and φ_1 . The zonal wind stress is integrated along three lines, (a) $\varphi = \varphi_1$, $0 < \lambda < \lambda_1$, (b) $\varphi = \varphi_2$, $\lambda_1 < \lambda < \lambda_2$, and (c) $\varphi = \varphi_1$, $\lambda_2 < \lambda < \lambda_0$. Equation (21) is similar to equation (32) in Ishida (1994), referred as (I-32) hereafter, who derived the wind-driven recirculation transport in the model basin with two partial meridional barriers overlapping each other under the planetary β approximation. To make clear the difference between (21) in this study and (I-32) derived in Ishida (1994), the latter is rewritten under spherical coordinates to lead

$$Q = [\tau^\lambda(\varphi_1) r \lambda_1 \cos \varphi_1 + \tau^\lambda(\varphi_2) r (\lambda_0 - \lambda_1) \cos \varphi_2] / (f_2 - f_1). \quad (22)$$

The comparison between (21) and (22) shows that the path of integration of wind stress is different in two cases. Figure 6 shows the stream lines of the recirculation (solid lines), and the paths of line integral of wind stress (dashed line). Although the stream lines are the same (PQRSP') in both cases with two meridional barriers (Fig. 6a) and with three meridional barriers (Fig. 6b), the paths of the line integral of wind stress is not the same. In the case of the basin with two meridional barriers, the line integral of the wind stress along the lines PS' and RQ' gives the driving force of the recirculation, as shown in Fig. 6a. On the other hand, for a basin with three meridional barriers, the paths of the line integral in the longitudinal band $0 < \lambda < \lambda_2$ are the lines PS' and RT', which are the same with two barriers, but the path in the band $\lambda_2 < \lambda < \lambda_0$ is the line UP'. Although the paths of wind stress integration are different in the two cases, the recirculation transports around the Antarctic Continent are derived from the same mechanism in which the recirculation is driven by the pressure difference at Drake Passage induced by the wind stress.

As stated above, the net recirculation transports in the two cases are not the same, even if the wind stress distribution is the same. However, since the scale of the distance between latitudes φ_1 and φ_2 is small compared with the scale of the wind stress distribution, the difference of the transports between the two cases is expected to be small.

The dependence of the recirculation transport on the wind stress distribution was also investigated. The wind stress is assumed to have the following distribution

$$\tau^\lambda(\varphi) = \cos [\pi (\varphi - \varphi_C) / \varphi_W], \quad (23)$$

where φ_C is the latitude of the maximum eastward wind stress, and φ_W is the meridional scale for the distribution. Figure 7 shows the recirculation transport Q as functions of φ_C and φ_W

The parameters of model geometry are given as follows: $\lambda_0=360^\circ$, $\lambda_1=30^\circ$, $\lambda_2=180^\circ$, $\varphi_1=57^\circ\text{S}$, and $\varphi_2=49^\circ\text{S}$. The recirculation transport is maximum when φ_c is near the mean latitude of φ_1 and φ_2 ($\varphi_c \approx 53^\circ\text{S}$). This is because the distance of the line integral at φ_1 , $r(\lambda_0 + \lambda_1 - \lambda_2)\cos\varphi_1 \approx 13000$ km, and the distance at φ_2 , $r(\lambda_2 - \lambda_1)\cos\varphi_2 \approx 11000$ km are nearly the same. The transport Q becomes larger as the scale φ_w becomes larger, and the transport is 195 Sv in the limit of infinity of φ_w . If the parameters of the wind stress distribution are given as the typical scales: $\varphi_c=47^\circ\text{S}$, $\varphi_w=40^\circ$ (Hellerman and Rosenstein, 1983), the transport Q is about 163 Sv. This value is slightly larger but is in the same order of the observed value 130 Sv being generally accepted (Whitworth *et al.*, 1982; Whitworth, 1983).

6. Discussion

The relation between the observed transport of the zonal current and the flux into or out of the Southern Ocean is discussed, applying the model results to observations. The buoyancy-driven component of the model ACC depends on the flux out of the Weddell Sea (S_w) much more than that into the Northern hemisphere ($S_A + S_P$) as described in Section 4. Table 1 shows the values of the proportional coefficients in (15) obtained by using the appropriate values of the basin parameters: $\varphi_1 = 57^\circ\text{S}$ and $\varphi_2 = 49^\circ\text{S}$. The magnitude of the flux S_w is critical to the transport of the model ACC, because inflow out of the Weddell Sea drives the westward current whose magnitude is about 7 to 9 times as large as S_w .

It is relevant to prescribe the transport of about 2 to 5 Sv of the bottom water out of the Weddell Sea, although the transport has been estimated in numerous studies with a wide range from 1 to 50 Sv (Solomon, 1974). Carmack and Foster (1975) suggested that the transport of the newly-formed bottom water is smaller than that estimated formerly, because the high values of the total transport out of the Weddell Sea estimated in some studies possibly include

a large fraction of Antarctic Bottom Water entering the Weddell Sea from the southeast. Foster and Carmack (1976) estimated a transport of 2 to 5 Sv from observed changes in bottom water properties between the southeastern and northwestern Weddell Sea. Weiss *et al.* (1979) obtained a transport of 2.9 Sv using tritium data. These low values seem to agree closely with the values estimated from dynamical considerations (Killworth, 1973; Gill, 1973).

If the transport of bottom water out of the Weddell Sea is about 3 Sv, the transports of the bottom zonal currents are given by about -21 to -27 Sv. This result does not represent the feature generally known that there is a mean eastward current in the deep layer rather than a westward current in the Southern Ocean (e.g. Gordon, 1966; Reid, 1986, 1989). However, some observations have shown bottom westward currents. Nowlin *et al.* (1977) showed a westward current through Drake Passage, using short-term current meter measurements to reference geostrophic calculations. Callahan (1971) also obtained a westward current with westward transport of about 24 Sv, using deep current measurement and hydrographic data in the Pacific sector. Whitworth *et al.* (1991) showed a current flows westward along the northern flank of the Falkland Plateau with mean westward transport of 8.2 Sv. They suggested that the observed bottom westward current is the southern boundary current in the Argentine Basin predicted by the Stommel-Arons model because the observed westward transport was larger than that into the Argentine Basin estimated by Georgi (1981). However, the Southern Ocean is not a closed basin in which the Stommel-Arons model can be applied in a straightforward manner. The model suggests that the bottom westward current observed by Whitworth *et al.* (1991) is a part of the zonally periodic recirculation shown in this model.

The current in the bottom layer is considered to be influenced by the bottom topography and not to be a simple zonal current like that shown in the model. However, it is reasonably

considered that the observed westward currents are driven by the mechanism shown in this model, because the model geometry is the most pronounced topography in the Southern Ocean and its effect on the circulation is expected to be large.

The deep current is also considered to be driven mainly by the flux between the Southern Ocean and the Weddell Sea. If the bottom water is formed by recooling of NADW (Broecker and Peng, 1982), the flux is given by $S_{w2} = -3$ Sv. Then the deep currents are eastward and the transports are given by about 21 to 27 Sv. The deep current is partially driven by the fluxes out of the North Atlantic and into the North Pacific, which are given by $S_{A2} = -14$ Sv and $S_{P2} = 10$ Sv according to estimates of Stommel and Arons (1960b). Thus the transports of the deep currents are about 30 Sv in the Atlantic sector and about 18 Sv in the Pacific sector. The transport in the Pacific sector is smaller than that in the Atlantic sector, because the transport in the Pacific sector given by (15) includes the flux S_p into the North Pacific.

It is well known in many observations that there is a mean eastward current in the deep layer. Kuo and Veronis (1973) and Kuo (1978) showed that a best fit of their model result to the observed oxygen was given, if the transport around the Antarctic Continent was fixed at 35 Sv. Rintoul (1991) showed that the net eastward transports through Drake Passage in the deep layer is about 44 Sv using hydrographic data and inverse methods. Although the deep eastward transport obtained in this model is smaller than these values, the magnitudes are of the same order. This suggests that the deep currents are driven mainly by the flux of the NADW into the Weddell Sea.

The transports of the buoyancy-driven currents in each layer are shown in Table 2, provided that the above estimates of the source and sink fluxes are given with the proportional coefficients shown in Table 1. The surface currents are expected to be driven mainly by the predominant eastward wind stress because the magnitude of the transports of the

buoyancy-driven currents is smaller than that of the wind-driven currents described in the previous section. We now describe the pattern of the interior circulation driven by both buoyancy and wind stress. Figure 8 shows the distributions of the surface deviation (Fig. 8a) and the interface deviation (Fig. 8b and c) in interior regions. The parameters of model geometry are the same as those used in Fig. 7, and the wind stress is given by (23). Then, the net eastward transport is 163 Sv as stated in the previous section. The transports Q_A , Q_B , and Q_C of the zonal boundary currents driven by wind stress at each sector are 142, 232, and 173Sv, respectively. The surface or interface deviations depend on the magnitudes of reduced gravity and layer thickness, and the following values are used: $(g_1, g_2, g_3) = (980, 2.0, 0.5) \text{ cm} \cdot \text{s}^{-1}$ and $(H_1, H_2, H_3) = (1, 2, 2) \text{ km}$.

Since the wind-driven circulation is predominant in the top layer, the distributions of the surface deviation η_1 and the interface deviation η_2 reflect the patterns of wind-driven circulation. On the other hand, the deviation η_3 reflects purely the patterns of buoyancy-driven circulation because the wind stress effects are restricted in the top layer. Since the circulations are derived in the limiting case with no friction in this study, the model ACC is represented as the zonal boundary currents with zero widths in three sectors. The interfacial gaps corresponding to the model ACC are found in Fig. 8. The order of the gap, i.e. the difference of interface deviation across the model ACC seems to be the same as that observed. The pattern of η_3 is similar to that described by Stommel and Arons (1960a), but the magnitude of η_3 is less than that of the interfacial gap by two orders. Thus, the zonal current is found to be predominant in the circulations in the Southern Ocean.

The wind stress drives the surface eastward current whose magnitude exceeds the westward buoyancy-driven component. The currents in the deep and bottom layers are eastward and westward, respectively, and are driven by buoyancy. Then it is found that the

vertical profile can be attributed to the surface wind-driven circulation and the deep and bottom buoyancy-driven circulation. Although the vertical profile can be explained qualitatively, the magnitude of the shear obtained by the model is larger than that observed. According to Rintoul (1991), the net eastward transports through Drake Passage in each layer are as follows: 85 Sv in the surface layer, 44 Sv in the deep layer, and 1 Sv in the bottom layer. The model of this study predicts the eastward transport in each layer to be 137, 31, and -27 Sv in order from the top layer, by using the parameters used in Fig. 8 and the fluxes S_w , S_A , and S_p in Table 2. The surface eastward transport obtained by the model is larger than that observed, and the deep eastward transport is smaller. The model bottom current is large westward, although the small eastward current is given in the analysis of observations. One reason of the difference between the model and the observed transport is that the model does not have variable depth. The magnitude of the bottom current transport will become smaller than that given above if the effect of variable depth is included, because the current is retarded by the bottom drag. Another is considered to be owing to that the model wind-driven circulation is restricted in the top layer because the linear and inviscid equations are used and no stress can be transferred across an interface. With regard to the prominence of eddies in the Southern Ocean (e.g. Patterson, 1985), Johnson and Bryden (1989) showed downward transfer of wind-imparted zonal momentum by eddy form drag using a simple model. Downward transfer also is shown as the result of eddy-resolving quasi-geostrophic models (McWilliams *et al.*, 1978; Treguier and McWilliams, 1990; Wolff and Olbers, 1989; Wolff *et al.*, 1991). If the mechanism of momentum exchange across an interface is included, the surface eastward momentum is transferred to the deep and bottom layers and the water will be accelerated eastward there.

7 Summary

The effects of three partial meridional barriers overlapping in a latitude band on the ACC have been investigated, especially the buoyancy-driven component, using a three-layer model. The model geometry is similar to that used by Ishida (1994) except that a third meridional barrier dividing the Pacific and the Indian basin was added. The transport of the buoyancy-driven component of the ACC in each layer is found to be given by (11) and (13). The transport can be expressed as a linear function of the transport S_w out of the Weddell Sea and the net northward transport $S_A + S_P$ into the Northern hemisphere across the equator. The zonal current flows westward if the fluxes S_w and $S_A + S_P$ are positive. The magnitude of the predominant term in equation (11) is inversely proportional to the difference between the Coriolis parameters at the latitudes of the ends of meridional barriers. The predominant term is proportional to S_x , which is part of the driving force of the buoyancy-driven zonal currents. The dependence of the zonal transport on S_w and $S_A + S_P$ is characterized by the ratio of the equatorial and polar area of the meridional barriers' overlapping latitude band. The transport of the zonal current depends on S_w more than $S_A + S_P$ by one order because the equatorial area is larger than the polar area by one order (see equation (14)).

It was found that the transport of the wind-driven component of the ACC is given by (21). The effects of the meridional barrier dividing the Pacific and the Indian Ocean are also investigated by comparing the result of this study with that of Ishida (1994). The difference between the results was found to be the latitude of the path of the line integral of zonal wind stress in the Pacific section. However, the wind-driven components of the ACC in two studies can be derived in the same mechanism, in which the recirculation around the Antarctic Continent is driven by the pressure difference across Drake Passage induced by wind stress.

The model results were applied to the real ocean based on observational data. The model

shows that the smaller estimates of the outflow from the Weddell Sea should be given to obtain an acceptable value of bottom current transport. The westward current is driven by the outflow from the Weddell Sea in the bottom layer. Although the bottom currents are considered to be influenced by the bottom topography and not to be simple zonal currents, the observed bottom westward currents are suggested to be driven by the mechanism shown in this model. The deep eastward transports obtained in this model are smaller than that shown in Kuo and Veronis (1973) and Rintoul (1991) but the magnitudes are of the same order.

The vertical shear of the ACC was found to be attributed to the surface wind-driven circulation and the deep and bottom buoyancy-driven circulation. Although the vertical structure is explained by the model qualitatively, the magnitude of the vertical shear obtained by the model is larger than that observed because wind effects are restricted in the top layer. It is because the linear equations and no stress transfer across an interface are assumed. The process of the momentum transfer across an interface should be included to describe the vertical structure of the ACC more realistically. However, the main objective of this paper was to illustrate the process how partial meridional barriers affect the transport and the structure of the ACC especially the buoyancy-driven component. It is left for future work to study the effects of bottom topography and the momentum exchange across an interface on the ACC.

Acknowledgements

I would like to express my thanks to Prof. N. Imasato of the Department of Geophysics for his guidance throughout and his valuable advice. I am also grateful to Dr. T. Awaji and Dr. K. Akitomo of the Department for their valuable comments and critical reading of the manuscript. Thanks are extended to other members of the Department of Geophysics of Kyoto University for their helpful discussions.

References

- Baker, D. J., Jr. (1982): A note on Sverdrup balance in the Southern Ocean. *J.Mar.Res.*, **40** (Suppl), 21-26.
- Broecker, W. S. and T.-H. Peng (1982): *Tracers in the sea*. Lamont-Doherty Geological Observatory, Columbia University, Palisades, New York, 690 pp.
- Callahan, J. E. (1971): Velocity structure and flux of the Antarctic Circumpolar Current south of Australia. *J.Geophys.Res.*, **76**, 5859-5864.
- Carmack, E. C. and T. D. Foster (1975): On the flow of water out of the Weddell Sea. *Deep-Sea Res.*, **22**, 711-724.
- Foster, T. D. and E. C. Carmack (1976): Frontal zone mixing and Antarctic Bottom Water formation in the southern Weddell Sea. *Deep-Sea Res.*, **23**, 301-317.
- Georgi, D. T. (1981): Circulation of bottom waters in the southwestern South Atlantic. *Deep-Sea Res.*, **28**, 959-979.
- Gill, A. E. (1968): A linear model of the Antarctic Circumpolar Current. *J.Fluid Mech.*, **32**, 465-488.
- Gill, A. E. (1973): Circulation and bottom water production in the Weddell Sea. *Deep-Sea Res.*, **20**, 111-140.
- Gordon, A. L. (1966): Potential temperature, oxygen and circulation of bottom water in the Southern Ocean. *Deep-Sea Res.*, **13**, 1125-1138.
- Hellerman, S. and M. Rosenstein (1983): Normal monthly wind stress over the world ocean with error estimates. *J.Phys.Oceanogr.*, **13**, 1093-1104.
- Hidaka, K. and M. Tsuchiya (1953): On the Antarctic Circumpolar Current. *J.Mar.Res.*, **12**, 214-222.
- Ishida, A. (1994): Effects of partial meridional barriers on the Antarctic Circumpolar Current

- Wind-driven barotropic model. *Dyn. Atmos.Oceans*. in press.
- Johnson, G.C. and H.L. Bryden (1989): On the size of the Antarctic Circumpolar Current. *Deep-Sea Res.*, **36**, 39-53.
- Johnson, J.A. and R.B. Hill (1975): A three-dimensional model of the Southern Ocean with bottom topography. *Deep-Sea Res.*, **22**, 745-751.
- Kawase, M. (1987): Establishment of deep ocean circulation driven by deep-water production. *J.Phys.Oceanogr.*, **17**, 2294-2317.
- Killworth, P. D. (1973): A two-dimensional model for the formation of Antarctic Bottom Water. *Deep-Sea Res.*, **20**, 941-971.
- Klinck, J.M. (1986): Channel dynamics and its application to the Antarctic Circumpolar Current. p. 299-328. In *Advanced Physical Oceanographic Numerical Modelling*, ed. by J.J. O'Brien, NATO ASI Series C, D. Reidel Publishing Company, Dordrecht.
- Kuo, H.H. (1978): Topographic effect on the deep circulation and the abyssal oxygen distribution. *J.Phys.Oceanogr.*, **8**, 428-436.
- Kuo, H.H. and G. Veronis (1973): The use of oxygen as a test for an abyssal circulation model. *Deep-Sea Res.*, **20**, 871-888.
- McWilliams, J.C., W.R. Holland and J.H.S. Chow (1978): A description of numerical Antarctic Circumpolar Currents. *Dyn.Atmos.Oceans.*, **2**, 213-291.
- Munk, W.H. and E. Palmén (1951): Note on the dynamics of the Antarctic Circumpolar Current. *Tellus*, **3**, 53-55.
- Nowlin, W.D., Jr., T. Whitworth, III and R.D. Pillsbury (1977): Structure and transport of the Antarctic Circumpolar Current at Drake Passage from short-term measurements. *J.Phys.Oceanogr.*, **7**, 788-802.
- Patterson, S.L. (1985): Surface circulation and kinetic energy distributions in the southern

- hemisphere oceans from FGGE drifting buoys, *J.Phys.Oceanogr.*, **15**, 865-884.
- Reid, J.L. (1986): On the total geostrophic circulation of the South Pacific Ocean: Flow patterns, tracers and transports. *Prog. Oceanog.*, **16**, 1-61.
- Reid, J.L. (1989): On the total geostrophic circulation of the South Atlantic Ocean: Flow patterns, tracers and transports. *Prog. Oceanog.*, **23**, 149-244.
- Rintoul, R.R. (1991): South Atlantic interbasin exchange. *J.Geophys.Res.*, **96**, 2675-2692.
- Solomon, H. (1974) : Comments on the Antarctic Bottom Water problem and high-latitude thermohaline sinking. *J.Geophys.Res.*, **79**, 881-884.
- Stommel, H. (1957): A survey of ocean current theory. *Deep-Sea Res.*, **4**, 149-184.
- Stommel, H. (1958): The abyssal circulation. *Deep-Sea Res.*, **5**, 80-82.
- Stommel, H. and A.B. Arons (1960a): On the abyssal circulation of the world ocean I. Stationary planetary flow patterns on a sphere. *Deep-Sea Res.*, **6**, 140-154.
- Stommel, H. and A.B. Arons (1960b): On the abyssal circulation of the world ocean II. An idealized model of the circulation pattern and amplitude in oceanic basins. *Deep-Sea Res.*, **6**, 217-233.
- Treguier, A.M. and J.C.McWilliams (1990): Topographic influences on wind-driven, stratified flow in a β - plane channel: An idealized model for the Antarctic Circumpolar Current. *J.Phys.Oceanogr.*, **20**, 321-343.
- Tziperman, E. (1986): On the role of interior mixing and air-sea fluxes in determining the stratification and circulation of the oceans. *J. Phys. Oceanogr.*, **16**, 680-693.
- Weiss, R.F., H.G. Ostlund and H. Craig (1979): Geochemical studies of the Weddell Sea. *Deep-Sea Res.*, **26**, 1093-1120.
- Whitworth, T., III, W.D. Nowlin, Jr. and S.J.Worley (1982): The net transport of the

- Antarctic Circumpolar Current through Drake Passage. *J.Phys.Oceanogr.*, **12**, 960-971.
- Whitworth, T., III (1983): Monitoring the transport of the Antarctic Circumpolar Current at Drake Passage. *J.Phys.Oceanogr.*, **13**, 2045-2057.
- Whitworth, T., III, W.D. Nowlin, Jr., R.D. Pillsbury, M.I. Moore and R.F. Weiss (1991): Observation of the Antarctic Circumpolar Current and deep boundary current in the Southwest Atlantic. *J. Geophys. Res.*, **96**, 15105-15118.
- Wolff, J.-O. and D.J. Olbers (1989): The dynamical balance of the Antarctic Circumpolar Current studied with an eddy resolving quasi-geostrophic model. p. 435-458. In *Mesoscale-synoptic coherent structures in geophysical turbulence*. ed. by J.C.J. Nihoul and B.M. Jamart, Elsevier, Amsterdam.
- Wolff, J.-O., E. Maier-Reimer and D.J.Olbers (1991): Wind-driven flow over topography in a zonal β -plane channel: A quasi-geostrophic model of the Antarctic Circumpolar Current. *J.Phys.Oceanogr.*, **21**, 236-264.

Table 1. The proportional coefficients (p_A , p_B , p_C , q_A , q_B , q_C) to the transports of the zonal currents in each section. The parameters of the model geometry are as follows: $\lambda_1=30^\circ$, $\lambda_2=180^\circ$, $\lambda_0=360^\circ$, $\varphi_1=57^\circ\text{S}$, $\varphi_2=49^\circ\text{S}$, $\varphi_0=70^\circ\text{S}$.

p_A	-8.9	q_A	-1.1
p_B	-7.2	q_B	-1.8
p_C	-8.1	q_C	-0.9

Table 2. The transports (S_w , S_A , and S_P) of the source/sink fluxes and the transports (Q_A , Q_B , and Q_C) of the zonal currents (Sv).

	S_w	S_A	S_P	Q_A	Q_B	Q_C
k = 1	0	14	-10	-4.4	-7.3	6.3
k = 2	-3	-14	10	31.1	28.8	17.9
k = 3	3	0	0	-26.6	-21.5	-24.2

Figure Captions

- Fig. 1 Schematic of the three-layer model with isopycnal heights (η_k), densities (ρ_k), mean layer thicknesses (H_k), and cross-isopycnal fluxes (w_{ij}) as indicated.
- Fig. 2 The geometry of the model. S_{wk} is the transport out of the Weddell Sea, and S_{Ak} and S_{Pk} are the transports into the North Atlantic and the North Pacific across the equator, respectively. Q_{Ak} , Q_{Bk} , and Q_{Ck} are the transports of the zonal boundary currents corresponding to the ACC.
- Fig. 3 The schematic view of zonal and western boundary currents driven by flux S out of the Weddell Sea into the North Atlantic (a), out of the Weddell Sea into the North Pacific (b), and out of the North Atlantic into the North Pacific (c).
- Fig. 4 The proportional coefficients p_A (a), p_B (b), and p_C (c) as functions of latitudes φ_1 and φ_2 . These values equal the transports Q_A , Q_B , and Q_C+S_p , respectively, when $S_w=1$, $S_A+S_p=0$.
- Fig. 5 The proportional coefficients q_A (a), q_B (b), and q_C (c) as functions of latitudes φ_1 and φ_2 . These values equal the transports Q_A , Q_B , and Q_C+S_p , respectively, when $S_w=0$, $S_A+S_p=1$.
- Fig. 6 The stream lines (solid lines) of the recirculation driven by wind, and the path of line integral (dashed line) of wind stress in the model basin with two meridional barriers (a) and with three meridional barriers (b). The points P', Q', R' and S' are located just west of points P, Q, R, and S across a meridional boundary.
- Fig. 7 The net eastward transport as a function of parameters φ_C and φ_w which characterize the wind stress distribution.
- Fig. 8 The distributions of interface deviations driven by surface wind stress and buoyancy. The wind stress distribution is given by equation (23). The transports into or out of the Southern Ocean are given in Table 2.

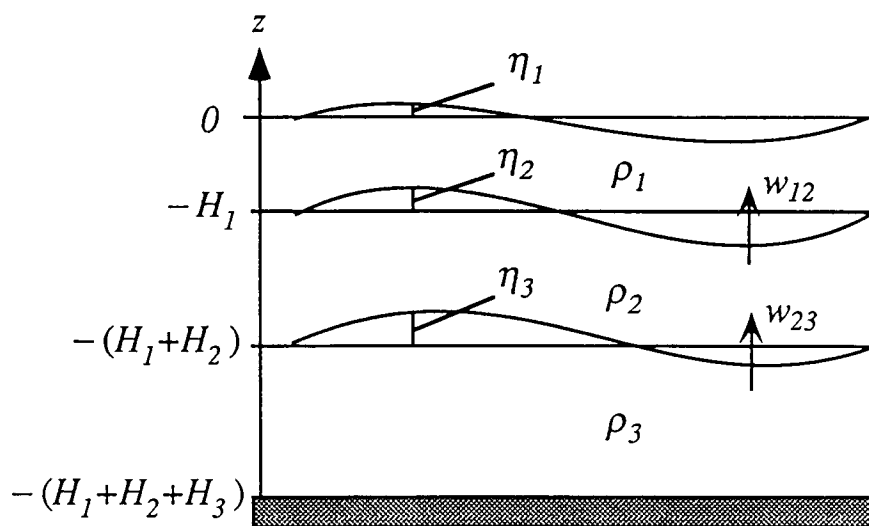


Fig 1 A Ishida

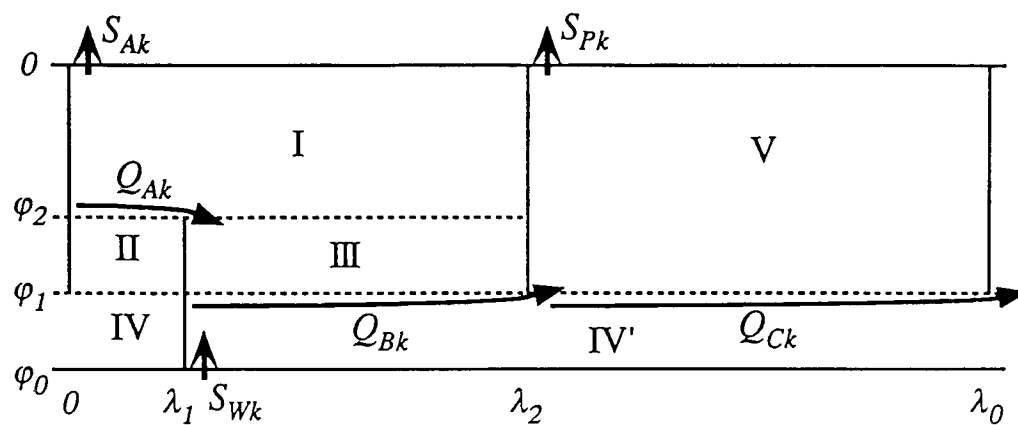


Fig. 2 A. Ishida

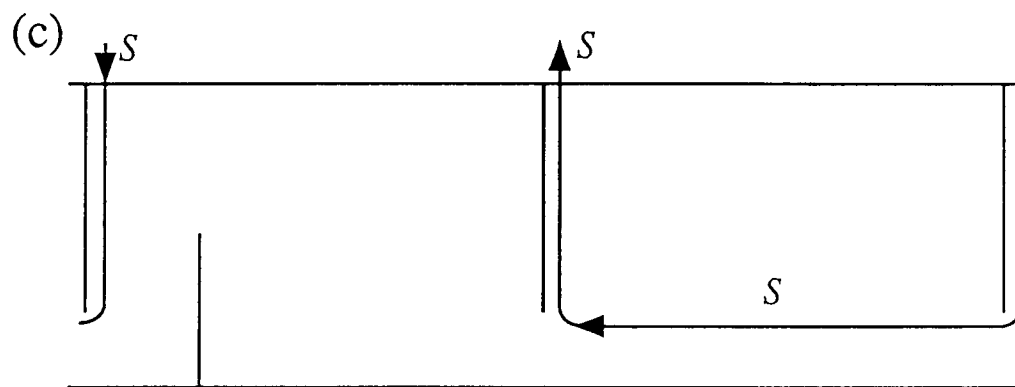
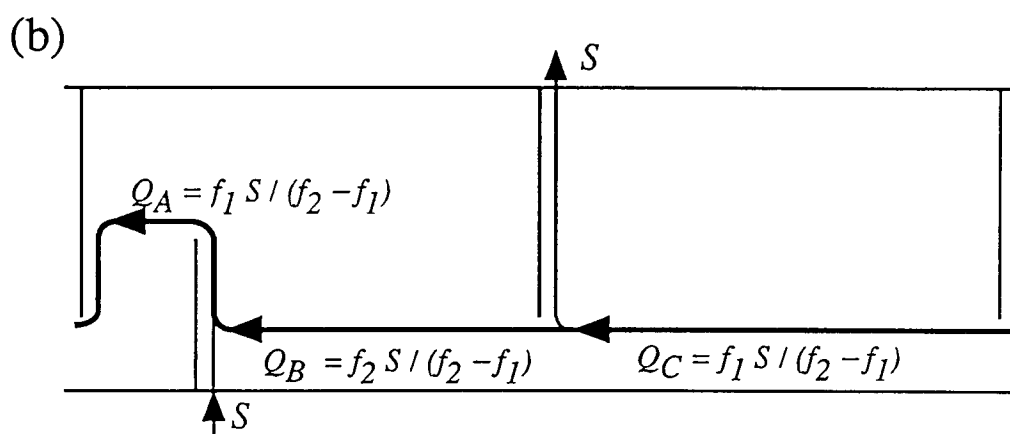
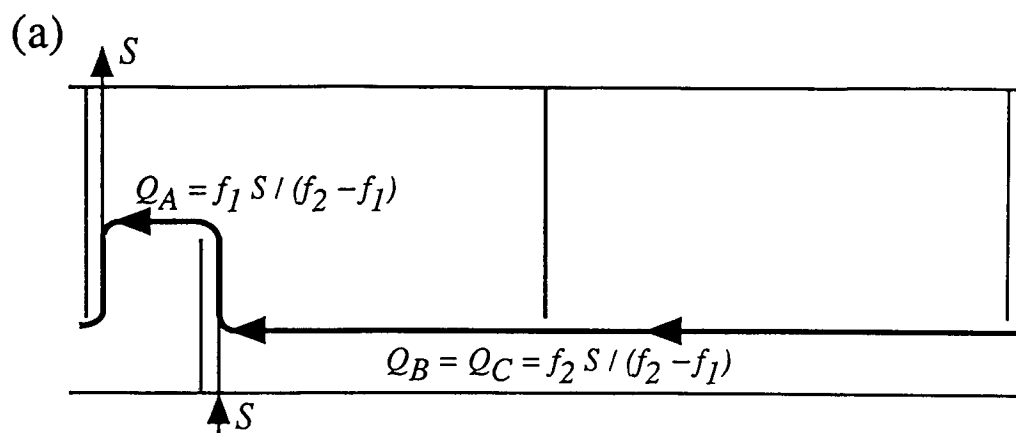


Fig. 3 A. Ishida

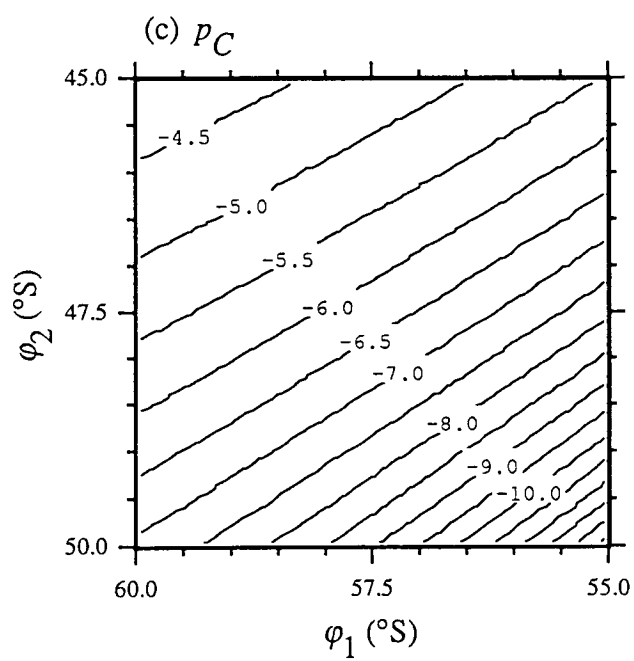
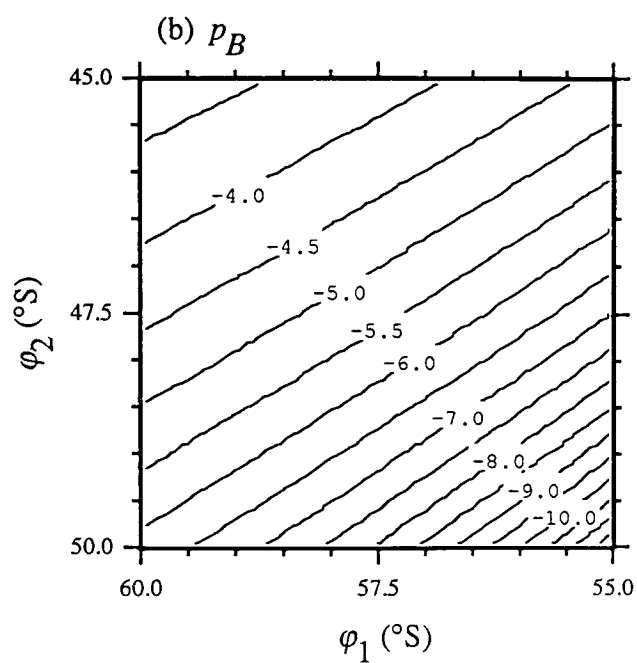
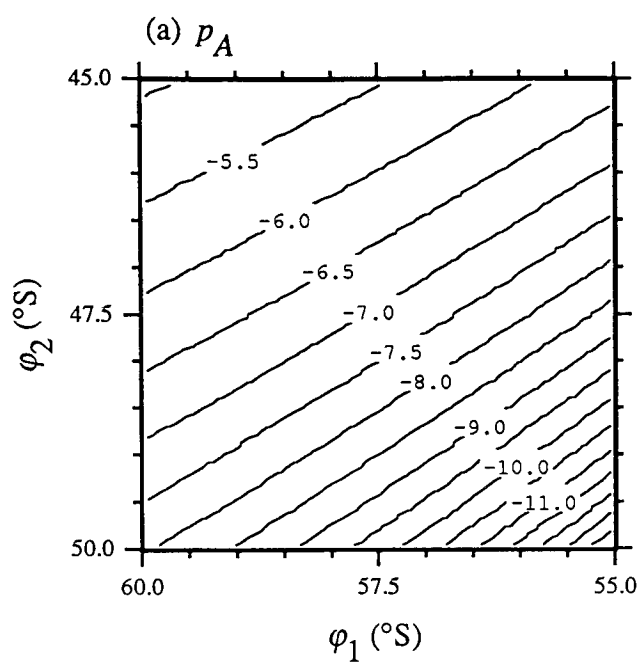


Fig 4 A Ishida

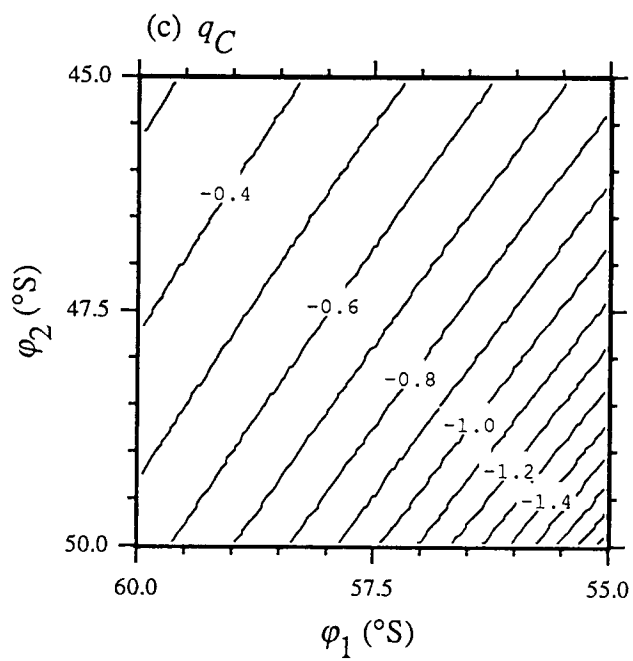
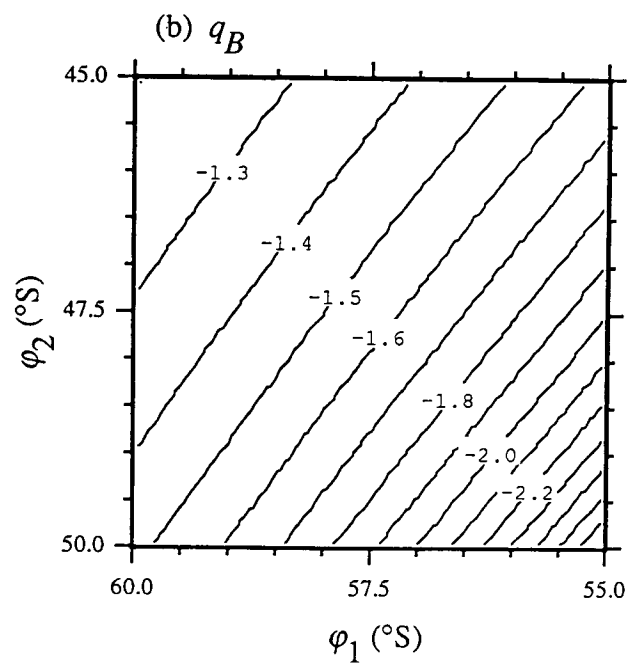
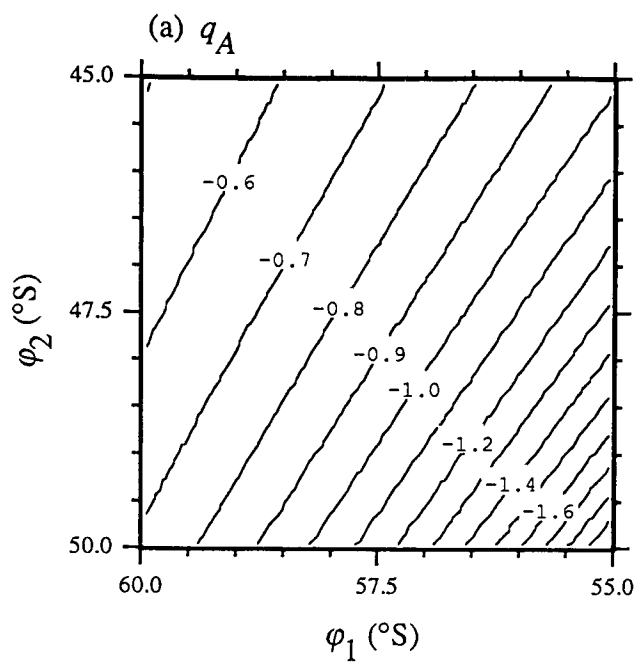
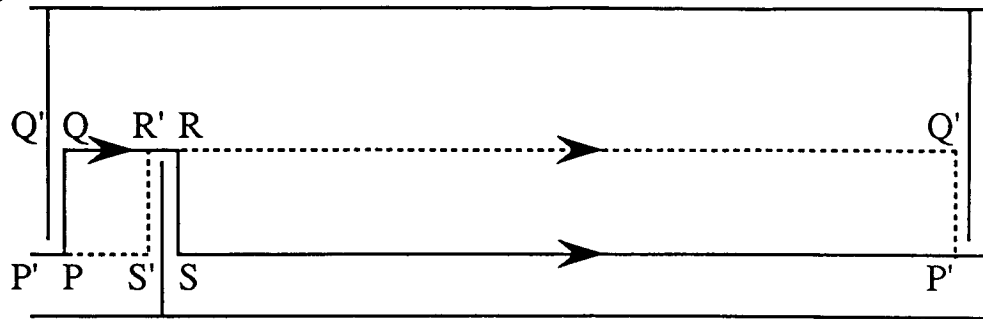


Fig. 5 A. Ishida

(a)



(b)

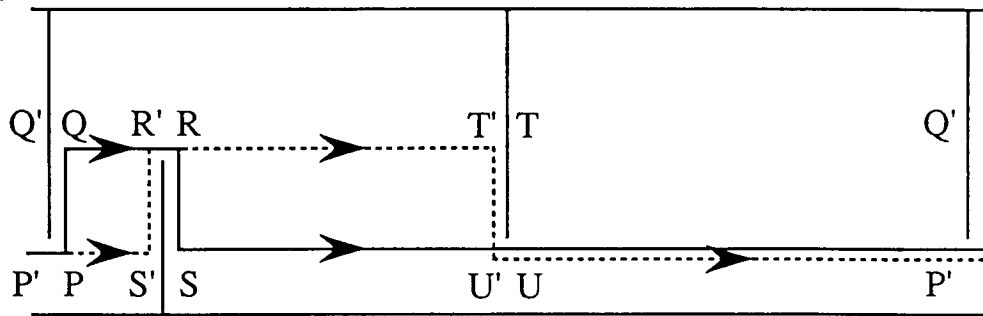


Fig. 6 A. Ishida

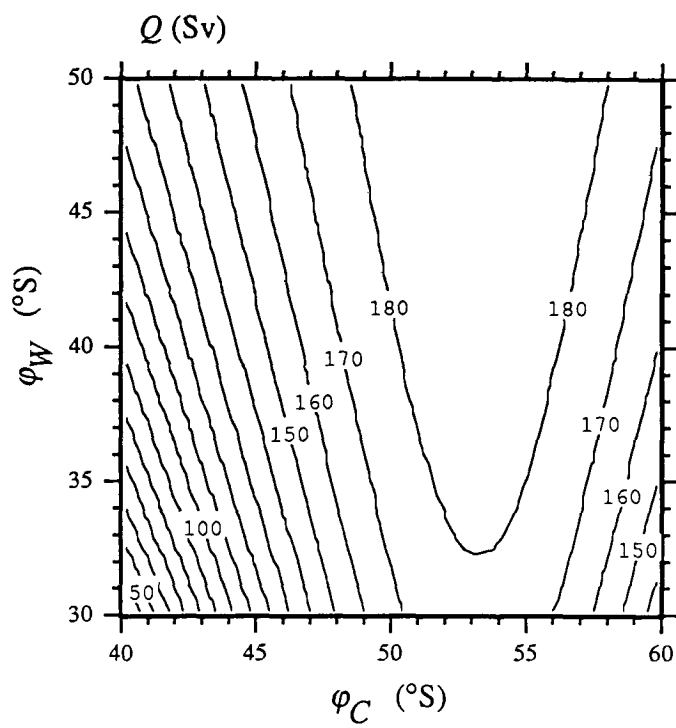


Fig. 7 A. Ishida

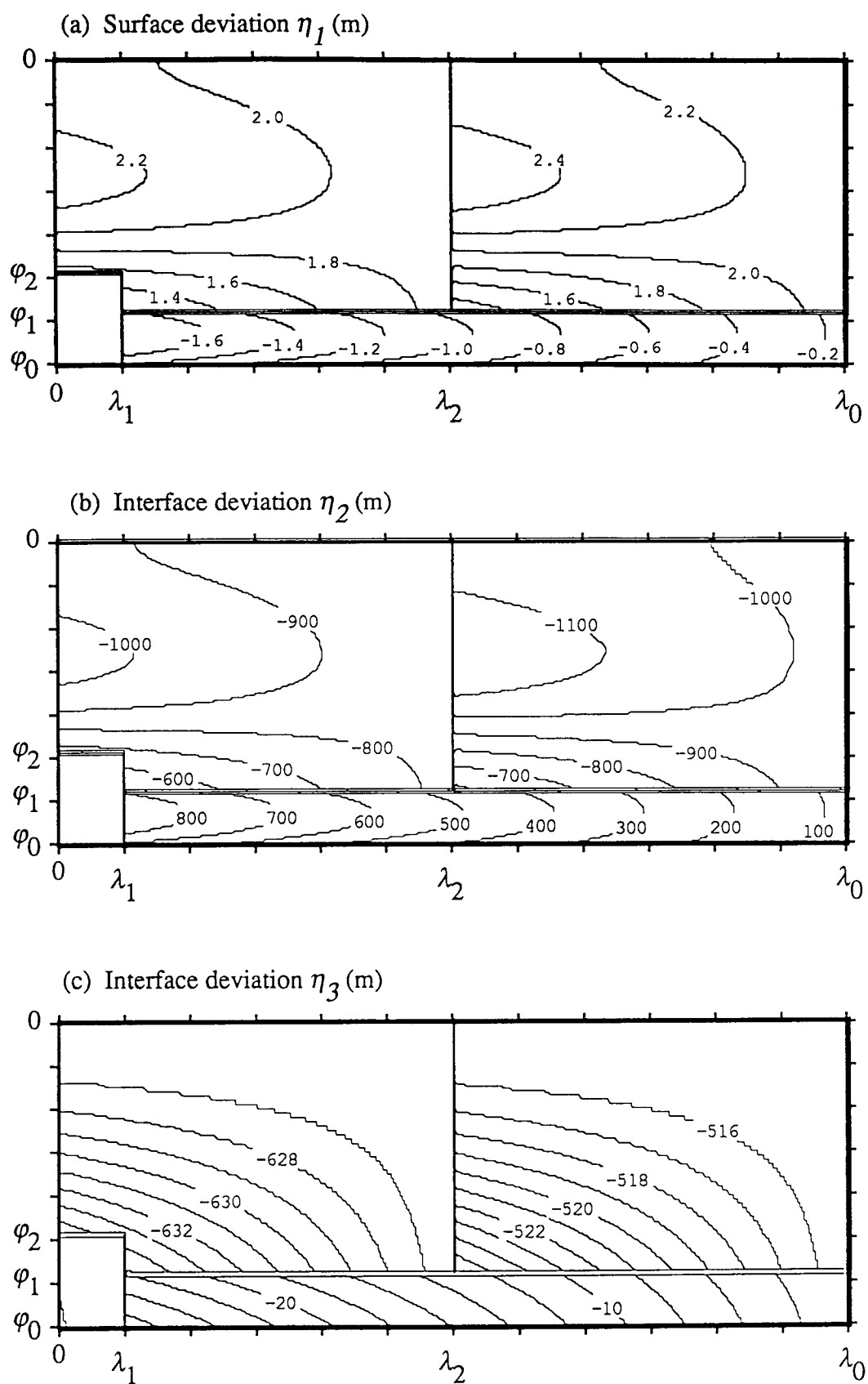


Fig. 8 A. Ishida